Reconstruction of warm season temperatures in central Europe during the past 60,000 years from lacustrine GDGTs

Paul D. Zander[1], Daniel Böhl[1], Frank Sirocko[2], Alexandra Auderset[1,3], Gerald Haug[1,4], Alfredo Martínez-García[1]

[1]Climate Geochemistry Department, Max Planck Institute for Chemistry, Mainz, 55128, Germany
[2]Institute of Geosciences, Johannes Gutenberg-University, Mainz, 55122, Germany
[3]School of Ocean and Earth Science, University of Southampton, Southampton SO14 3ZH, United Kingdom
[4]Department of Earth Sciences, ETH Zurich, Zurich, 8092, Switzerland

Correspondence to: Paul D. Zander (paul.zander@mpic.de)

Abstract

Millennial-scale climate variations during the last glacial period, such as Dansgaard–Oeschger (D/ODO) cycles and Heinrich events, have been extensively studied using ice core and marine proxy records. However, there is a limited understanding of the magnitude of these temperature fluctuations in continental regions, and questions remain about the seasonal signal of these climate events. This study presents a 60,000-year long temperature reconstruction based on branched glycerol dialkyl glycerol tetraethers (brGDGTs) extracted from lake sediments from the Eifel volcanic field, Germany. brGDGTs are bacterial membrane-spanning lipids that are known to have a strong relationship with temperature, making them suitable for temperature reconstructions. We test several temperature calibration models on modern samples taken from soils and multiple maar lakes. We find a bias associated with water depth and anoxic conditions that can be corrected for by accounting for a brGDGT isomer that is only produced in anoxic conditions. The corrected temperature reconstruction correlates with proxy and climate model temperature recordestimates of temperature spanning the same time period, validating the calibration modelapproach we selected. However, millennial-scale variability is significantly dampened in the brGDGT record, and in contrast to other northern hemisphere climate records, during several Heinrich stadials, temperatures actually increase. We demonstrate that these apparent discrepancies can be explained by the unique seasonal response of the brGDGT paleothermometer to temperatures of months above freezing (TMAF). Our data support the view that warm season temperatures in Europe varied minimally during the last glacial period, and that abrupt millennial-scale events were defined by colder, longer winters. Our continuous high-resolution temperature reconstruction provides important information about the magnitude of seasonal climate variability during the last glacial period that can be used to test climate models and inform studies of paleoecological change.

1 Introduction

Millennial-scale climate variations during the last glacial period (Dansgaard–Oeschger (D/ODO) cycles and Heinrich events) are well documented in ice core and marine proxy records (Rasmussen et al., 2014; Davtian and Bard, 2023; Martrat et al.,

2007; Dansgaard et al., 1993). Abrupt warming is recorded within decades in ice cores at the onset of Greenland interstadials (GIs), followed by gradual cooling, forming a repeated saw-shaped pattern (Rasmussen et al., 2014; North Greenland Ice Core Project members, 2004). Coarse-grained layers of ice-rafted debris in the North Atlantic are markers of Heinrich events (Heinrich, 1988), which are associated with pronounced declines in sea surface temperatures and major changes in oceanographic conditions, including weakened Atlantic Meridional Overturning Circulation (AMOC) (Martrat et al., 2007; Davtian and Bard, 2023; Bohm et al., 2015) and expanded sea ice in the North Atlantic (De Vernal et al., 2006). Millennial-scale climate events can be detected in terrestrial records from Europe during the last glacial period including lake sediments and paleoecological records (Duprat-Oualid et al., 2017; Guiot et al., 1993; Wohlfarth et al., 2008; Ampel et al., 2010; Fletcher et al., 2010), loess (Prud'homme et al., 2022; Újvári et al., 2017), and speleothems (Genty et al., 2003; Spötl and Mangini, 2002; Genty et al., 2010). Pollen deposited in marine sediment cores off the coast of the Iberian peninsula and France confirm that these millennial-scale events occurred in Europe synchronously with oceanographic changes (Sánchez Goñi et al., 2000, 2008). Yet, there is a lack of continuous quantitative estimates of temperature fluctuations across these events from ~~continental regions~~the European continent, limiting our understanding of the magnitude of potential millennial scale climate variability ~~on continents~~in terrestrial environments. The sparse proxy data leads to divergent interpretations of the magnitude of temperature change associated with these millennial-scale events ~~.~~and, in particular, the role of changing seasonal conditions in driving observed changes in proxy records.

Glycerol dialkyl glycerol tetraethers (GDGTs) provide a unique opportunity to quantitatively estimate past temperatures over continental regions. Branched GDGTs (brGDGTs) are bacterial membrane lipids and are found in a wide range of environments including lakes, soils, loess, and marine environments (Hopmans et al., 2004; Schouten et al., 2013; De Jonge et al., 2014; Xiao et al., 2016; Raberg et al., 2022). The source organisms for these lipids are not well-constrained, however recent research has shown that certain strains of Acidobacteria produce brGDGTs in culture (Halamka et al., 2023; Chen et al., 2022; Sinninghe Damsté et al., 2011~~, p.1~~). Temperature has repeatedly been shown to drive brGDGT distributions, particularly the degree of methylation, and this relationship can be demonstrated in laboratory experiments (Martínez-Sosa et al., 2020; Martínez-Sosa and Tierney, 2019; Halamka et al., 2023), global datasets (Raberg et al., 2022, 2021; Martínez-Sosa et al., 2021; Naafs et al., 2017; Dearing Crampton-Flood et al., 2020; Weijers et al., 2007; De Jonge et al., 2014; Russell et al., 2018), and through *in situ* monitoring (Zhao et al., 2021). brGDGTs preserved in lake sediments can provide continuous, high-resolution records of past temperatures, and research in recent years has focused on expanding global calibration datasets for the lacustrine brGDGT paleothermometer. Initial studies interpreted brGDGTs in lacustrine sediments as derived from soil (Hopmans et al., 2004); however it is now established that the majority of lacustrine brGDGTs are produced within the aquatic environment (Bechtel et al., 2010; Tierney and Russell, 2009; Tierney et al., 2010; Van Bree et al., 2020; Weber et al., 2018, 2015; Zhao et al., 2021; Wang et al., 2023). Recent global calibrations have shown that brGDGTs are sensitive to the temperature of months above freezing (TMAF), likely because bacterial growth is substantially lower below freezing temperatures, and ice cover on lakes disconnects lacustrine brGDGT producers from atmospheric conditions (Dearing

65 Crampton-Flood et al., 2020; Martínez-Sosa et al., 2021; Raberg et al., 2021; Cao et al., 2020). The two most recent lacustrine brGDGT-temperature calibrations have errors of 2.1-2.9 °C across a diverse set of lakes spanning the globe (Raberg et al., 2021; Martínez-Sosa et al., 2021), proving this proxy can effectively be utilized for quantitative past temperature reconstructions.

70 Despite the ubiquitous relationship between temperature and brGDGT distributions, challenges remain for interpreting paleoclimate records from brGDGTs. Factors other than temperature are known to affect brGDGT distributions, which may lead to biases in temperature reconstructions. These non-climatic factors include oxygen/water depth (Weber et al., 2018, 2015; Van Bree et al., 2020; Halamka et al., 2023; Stefanescu et al., 2021), salinity (Wang et al., 2021), pH (De Jonge et al., 2014; Parish et al., 2023; Martínez-Sosa and Tierney, 2019), and conductivity (Raberg et al., 2021). Furthermore, changes in the
75 sources of brGDGTs can dramatically impact temperature reconstructions; brGDGTs produced in soils will produce a warm bias when input to a lacustrine calibration equation (Ramos-Román et al., 2022; Martin et al., 2020). Within lake variations in bacterial communities could also produce different temperature signals, with a cold bias from GDGTs produced at depths below the thermocline (Van Bree et al., 2020; Weber et al., 2018; Stefanescu et al., 2021; Sinninghe Damsté et al., 2022).

80 In this study, we measured brGDGTs in a composite lake sediment record from Eifel maar lakes (Sirocko et al., 2021) to reconstruct TMAF at multi-centennial resolution. Modern samples were utilized to test brGDGT-temperature calibrations, and we use an isomer that is only produced in anoxic settings to correct for biases that occur when a large portion of brGDGTs are produced in the hypolimnion of stratified lakes. The temperature record provides a unique insight into millennial scale climate variability and changing seasonal temperature gradients in central Europe during the past 60,000 years.

85 **2 Methods and materials**

2.1 Study area and sample collection

The Eifel volcanic field of western Germany features more than 250 Quaternary age scoria cones (Schmincke, 2007), and is well known for its maar basins, seven of which are currently lakes, while another >60 have been filled with sediments (Sirocko, 2016). The modern climate of the region is a temperate oceanic climate (Cfb) with cool winters (mean Jan temperature = 0
90 °C), warm summers (mean July temperature = 16 °C), and precipitation distributed throughout the year (mean annual precipitation = 817 mm) (Deutscher Wetterdienst, Climate Data Center). The modern landscape is a mosaic of agricultural areas, urban land use, and patches of deciduous broad-leaved forests or mixed coniferous broad-leafed forests.

The Eifel Laminated Sediment Archive (ELSA) project has systematically drilled maar features in the Eifel (Sirocko, 2016).
95 Five maar sites (Table 1Table 1; Figure 1Figure 1) are relevant for the current study: Auel (dry) Maar (AU), Gemündener Maar (GM), Weinfelder Maar (WM), Holzmaar (HM), and Schalkenmehrener Maar (SM). Sediment cores obtained from Auel

Maar (AU3, AU4), Holzmaar (HM3, HM4), and Schalkenmehrener Maar (SMF1, SMF2) were used to build a continuous 60,000 year record (ELSA-20 stack), which has previously been investigated for changes in vegetation (Sirocko et al., 2016, 2022), lake productivity (Sirocko et al., 2021), floods (Brunck et al., 2016), and dust (Fuhrmann et al., 2021). The chronology for the ELSA-20 stack is based on a combination of varve counts, marker layers, pollen stratigraphy, radiocarbon ages and tuning of high-resolution C_{org} data with the NGRIP $\delta^{18}O$ record (Sirocko et al., 2021, 2022). For our downcore analysis of GDGTs, 317 samples were analyzed, with each sample typically spanning 10 cm. On average (median), each sample represents ~43 years, and the interval between each sample midpoint is 116 years (range 14-1380 yr); the temporal resolution is lower for the period 24,000 yr b2k (years before 2000 CE) to present. Samples from Auel Maar represent the period 58,340-14,300 yr b2k, Holzmaar represents 14,200-690 yr b2k, and Schalkenmehrener Maar represents 630-0 yr b2k.
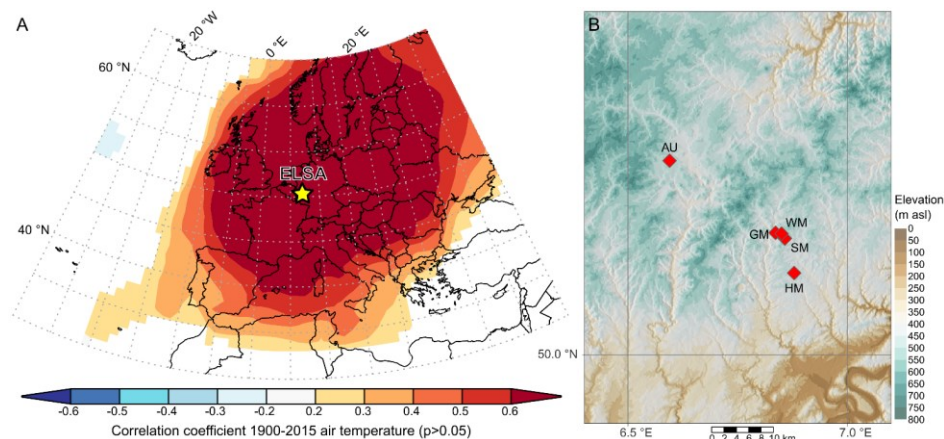
Figure 1: Location map. A) Spatial correlation of annual temperature at ELSA site compared with regional surface temperatures over the period 1900-2015. Data from NOAA-CIRES-DOE 20th Century Reanalysis V3 (Compo et al., 2011; Slivinski et al., 2019). B) Topographic map of sample sites for this study. AU= Auel Maar, GM = Gemündener Maar, WM = Weinfelder Maar, HM = Holzmaar, SM = Schalkenmehrener Maar. Topographic data from naturalearthdata.com.

Table 1: Summary of study sites and their properties. MAAT = Mean Annual Air Temperature and TMAF = Temperature of Months above Freezing. Temperature data refers to 1901-2016 period from CRU TS v4.01 dataset (Osborn and Jones, 2014).

Lake	ID	Longitude	Latitude	Altitude [m asl]	Water depth [m]	Diameter [m]	MAAT [°C]	TMAF [°C]	Soil	Lake surface	Lake core
Auel dry Maar	AU	6.59502	50.2826	456	-	1325	8.01	8.77	-	-	285
Holzmaar	HM	6.87866	50.1191	425	21	272	8.22	8.97	4	4	39
Schalkenmehrener Maar	SM	6.85766	50.1694	420	21	528	8.25	9.00	4	18	15
Gemündener Maar	GM	6.83631	50.1777	407	38	309	8.34	9.09	3	-	2
Weinfelder Maar	WM	6.84997	50.1765	484	51	525	7.83	8.58	2	-	-

Modern samples of soils (n = 13) were taken from the vicinity of Gemündener Maar, Weinfelder Maar, Holzmaar, and Schalkenmehrener Maar. Lake surface sediments were also taken from Holzmaar, and Schalkenmehrener Maar; each surface sediment sample represents approximately the upper 4 cm of sediment. Four samples were taken from 19 m water depth in Holzmaar, while a depth transect from 0.5-21.7 m water depth was obtained at Schalkenmehrener Maar (n = 18). Additionally, 13 samples from the upper 50 cm (representing sediments younger than 1900 CE) of sediment cores retrieved from Gemündener Maar, Holzmaar, and Schalkenmehrener Maar were included in the modern set of samples (total of 48 samples) that were used to test GDGT calibrations against modern climate data.

2.2 X-ray fluorescence core scanning

Sediment cores from Holzmaar (HM4) and Auel Maar (AU4) were scanned with an Avaatech X-ray fluorescence (XRF) core scanner (Avaatech XRF Technology) at the Max Planck Institute for Chemistry in Mainz to obtain semi-quantitative elemental data. The core face was smoothed and flattened using a blade, then covered with 4-μm-thin SPEX CertiPrep Ultralene film to avoid contamination and drying during measurements. XRF scans were performed using a rhodium anode tube with a voltage of 10 kV, a current of 550 μA, and counting time of 10 s. The measurement resolution was 0.5 mm. We utilize the counts of Ti as an indicator of terrigenous clastic sediment input, and the ratio of S/Ti as an indicator of hypolimnetic anoxia or sediment anoxia.

2.3 GDGT extraction and measurement

Samples were freeze-dried, homogenized, and then extracted using an accelerated solvent extractor (ASE) following the two-fraction method for lake sediments and soil of (Auderset et al., (2020). Between 0.2 and 3.51 g of dried sediment was weighed into an ASE cell with approximately 16 g of silica gel, which had previously been baked at 500 °C for 5 hours, then deactivated with 5% Milli-Q water and stored in *n*-hexane. A two-step extraction was performed with *n*-hexane and a 1:1 dichloromethane/methanol mix, which were flushed through the cells at 100 °C and 100 bar. The dichloromethane/methanol fraction contains the GDGT molecules. After extraction, a known amount (~700 ng) of internal C_{46} GDGT standard (Patwardhan and Thompson, 1999) was added to the extracts. Solvents were then evaporated with a low-pressure centrifuge (Rocket by Genevac). Samples were re-dissolved in ~1 ml of a 98.5:1.5 mix of *n*-hexane/2-propanol and filtered with 0.4 μm PTFE filters. SubqequentlySubsequently, solvents were evaporated using a FlexiVap and samples re-dissolved in 300 μl of 9:1 *n*-hexane/2-propanol, or a greater volume for particularly concentrated samples.

GDGTs were measured with an Agilent 1260 Infinity HPLC-MS (High Performance Liquid Chromatography Mass Spectrometer). The HPLC method was based on (Hopmans et al., 2016) and used a flow of 0.2 ml/min of 9:1 *n*-hexane/2-propanol through a silica column (UPLC BEH HILIC, 1.7μm) at 200 bar. Five μl were injected from each sample. A North Atlantic Standard (Auderset et al., 2020) was run with each sample batch for quality control and to identify individual GDGT

145 compounds. Data evaluation and peak integration was performed using Agilent MassHunter. The standard set of isoprenoid and brGDGT compounds were identified based on (Hopmans et al., 2016), and an additional isomer, IIIa'', which is specifically produced under low oxygen conditions, was also identified (Weber et al., 2018, 2015). The limit of detection of each measured compound was determined using the method defined by (Currie, (1999) (eq. 14) based on the repeated (n = 17) analysis of method blanks. The reproducibility of the method was assessed by repeated (n = 17) extraction and measurement

150 of a single sediment sample (Table S1).

2.4 Temperature calibration and data analysis

Several calibration models exist for transforming brGDGT fractional abundances into temperature estimates, and the different calibrations can yield substantially different results. We tested several calibration models on our set of modern samples to assess their ability to produce temperatures that agree with instrumental temperatures. We used the CRU TS v4.01 dataset for

155 modern temperature (representing the period 1901-2016; (Osborn and Jones, 2014)). We corrected for elevation differences at the five sample sites using a lapse rate of 6.6 °C/km calculated from nearby meteorological stations (German Weather Service). The altitude correction was also applied to reconstructed temperatures to ensure a homogenous reconstruction that represents the temperature at Auel Maar (465 m above sea level; asl).

160 The following calibration models were assessed. We calculated

- mMean annual air temperatures (MAAT) using the soil-based calibrations of De Jonge et al. (2014) using the MBT'$_{5Me}$ index and Index 1, respectively:

$$MBT'_{5Me} = \frac{Ia + Ib + Ic}{Ia + Ib + Ic + IIa + IIb + IIc + IIIa}$$ (1)

165

$$MBT'_{5Me}\ Soil\ MAAT = -8.57 + 31.45 * MBT'_{5ME}$$ (2)

$$Index\ 1 = log_{10}\frac{Ia + Ib + Ic + IIa' + IIIa'}{(Ic + IIa + IIc + IIIa + IIIa')}$$ (3)

170 $$Index\ 1\ Soil\ MAAT = 5.05 + 14.86 * Index\ 1$$ (4)

- We also calculated the Bayesian calibration models, BayMBT, for soils (Dearing Crampton-Flood et al., 2020) and lakes (Martínez-Sosa et al., 2021), which are based on the MBT'$_{5Me}$ index and calibrated for TMAF (Temperature of Months Above Freezing). We calculated temperatures using the

175 - FROG$_0$ (random **F**orest **R**egression for Pale**O**MAAT using br**G**DGTs) calibration model for soils (Véquaud et al., 2022). We calculated temperatures from the

- African lakes calibration models from Russell et al. (2018) using Index 1 and stepwise forward selection multivariate regression:

$$Index\ 1\ Lake\ MAAT\ =\ 12.22\ +\ 18.79 * Index\ 1 \tag{5}$$

~~and stepwise forward selection multivariate regression:~~

$$SFS\ Lake\ MAAT\ =\ 23.81 -\ 31.02 * IIIa - 41.91 * IIb - 51.59 * IIb' - 24.70 * IIa + 68.80 * Ib \tag{6}$$

- ~~We calculated temperatures using t~~The multivariate calibration model of Raberg et al. (2021), hereafter referred to as Raberg21:

$$Raberg21\ Lake\ TMAF\ =\ 92.9(\pm15.98) + 63.84(\pm15.58) * flb_{Meth}^2 - 130.51(\pm30.73) * flb_{Meth} - 28.77(\pm5.44) * fIIa_{Meth}^2 - 72.28(\pm17.38) \cdot fIIb_{Meth}^2 - 5.88(\pm1.36) \cdot fIIc_{Meth}^2 + 20.89(\pm7.69) \cdot fIIIa_{Meth}^2 - 40.54(\pm5.89) \cdot fIIIa_{Meth} - 80.47(\pm19.19) \cdot fIIIb_{Meth} \tag{7},$$

where the compound fractions are calculated according to their methylation set; see Raberg et al. (2021) for details.

To assess how brGDGT distributions varied in different types of samples and different sites, a principal component analysis (PCA) was calculated on the fractional abundances of brGDGTs; the FAs were calculated as centered-log ratios and scaled prior to the PCA calculation. To assess changing sources of GDGTs we calculated several indices. The $\Sigma IIIa/\Sigma IIa$ ratio was modified from Xiao et al. (2016) and Martin et al. (2019), and has been used as an indicator of aquatic production of brGDGTs:

$$\frac{\Sigma IIIa}{\Sigma IIa} = \frac{IIIa + IIIa' + IIIa''}{IIa + IIa''} \tag{8}$$

The branched and isoprenoid tetraether index (BIT) compares the proportion of branched GDGTs to the crenarchaeol, and has been used as an indicator of soil input (Hopmans et al., 2004, 2016):

$$BIT = \frac{Ia + IIa + IIa' + IIIa + IIIa'}{Ia + IIa + IIa' + IIIa + IIIa' + Crenarchaeol} \tag{9}$$

The %GDGT-0 index was calculated using the formula of (Peaple et al., 2022) and used as an indicator of anaerobic methane-oxidizing archaea or methanogenic Euryarchaeota (Sinninghe Damsté et al., 2012).

210

$$\%GDGT-0 = \frac{GDGT-0}{GDGT-0+Crenarchaeol} * 100 \qquad (10)$$

Statistical analyses were performed in R v4.3 (R Core Team, 2022). Pearson's r was used to assess the strength of correlations between timeseries and was calculated using the package GeoChronr (Mckay et al., 2021). Timeseries data were mapped to a
215 normal distribution; p-values were adjusted to ~~take into~~ account for autocorrelation using the effective n method (Dawdy and Matalas, 1964) and were adjusted for multiple hypothesis testing using the false discovery rate method of Benjamini and Hochberg (1995).

3. Results and discussion

3.1 GDGT distribution in modern samples and implications for temperature calibrations

220 The compositions of brGDGTs in modern samples shows clear differences between samples taken from soils and lake sediments (Figure 2~~Figure 2~~, Figure 3~~Figure 3~~). Soils have a greater proportion of tetra-methylated (Ia-c) GDGTs as well as IIa and IIa'. The hexamethylated compounds IIIa, IIIa', IIIa'', IIIb, and IIIb' are less abundant in soils. The samples taken from the shallow lake shore (depths < 1 m) have a composition that falls between soil and lake sediment. The IIIa'' isomer is not found above the limit of detection in any of the soil samples, but is found in all of the modern and ancient lake sediments,
225 with the exception of two samples from Auel maar dating to the last deglaciation. The modern lake sediments tend to have generally similar distributions compared to each other, however, some small differences can be observed. SM has less tetra-methylated GDGTs and more IIIa'' indicating a dominance of aquatic production, and particularly high production within the anoxic hypolimnion. A strong relationship can be observed between fIIIa'' and depth in the transect from Schalkenmehrener Maar (Figure 4~~Figure 4~~), consistent with previous studies that have concluded this isomer is produced under low oxygen
230 conditions (Weber et al., 2018, 2015).
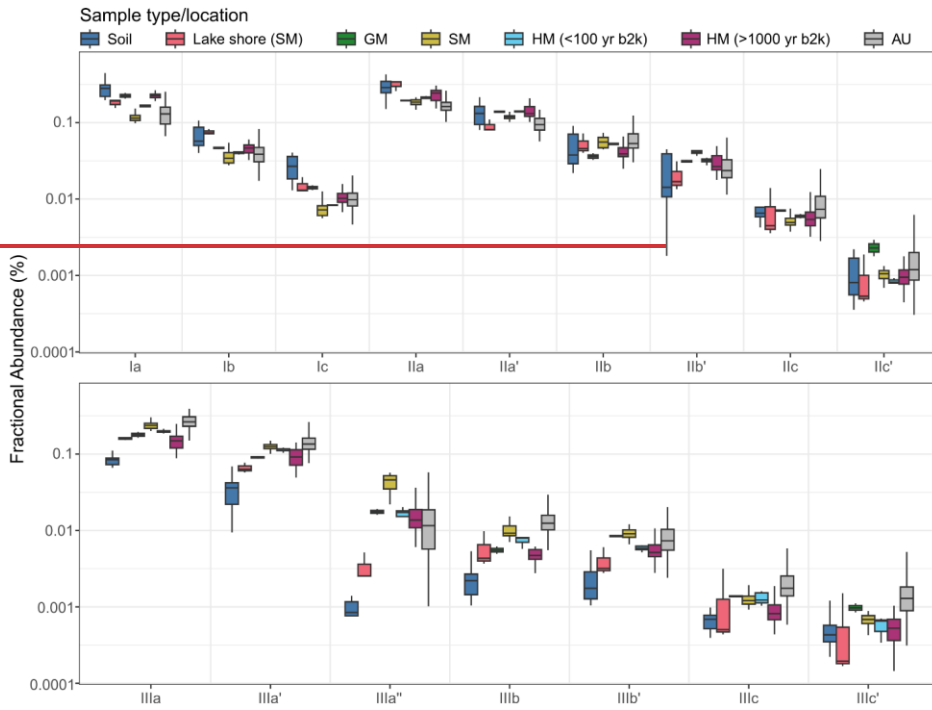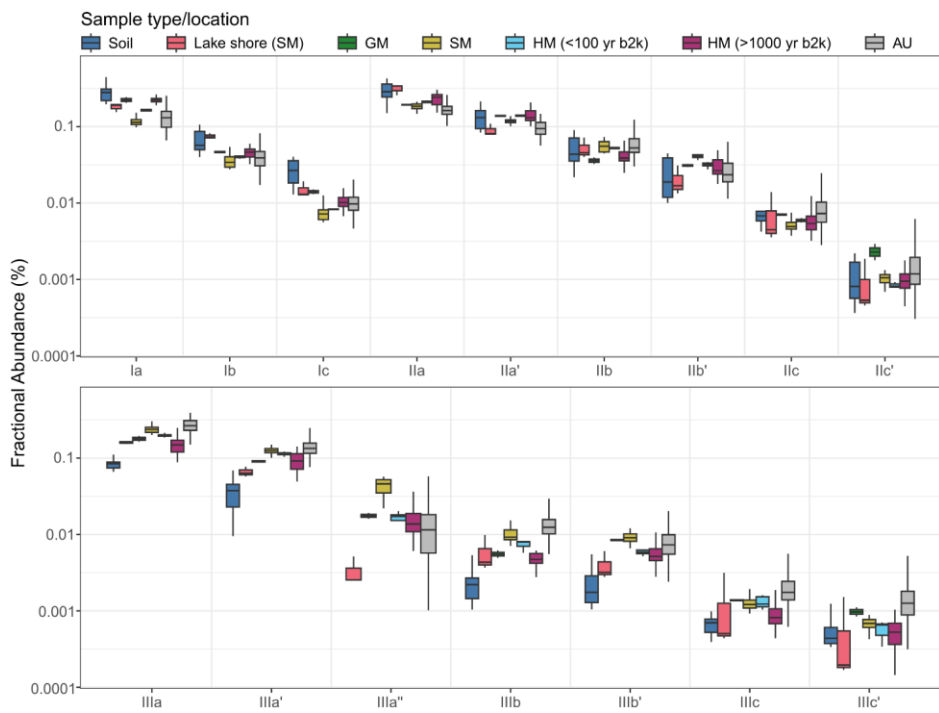
Figure 2: Distribution of brGDGT compounds at different sites (for abbreviations see Figure 1) and among different sample types. Boxes represent the interquartile range (IQR) of the data, with the median depicted by a horizontal line. Whiskers represent the minimum and maximum of the data, excluding outliers that are greater than 1.5 times the IQR beyond the IQR.
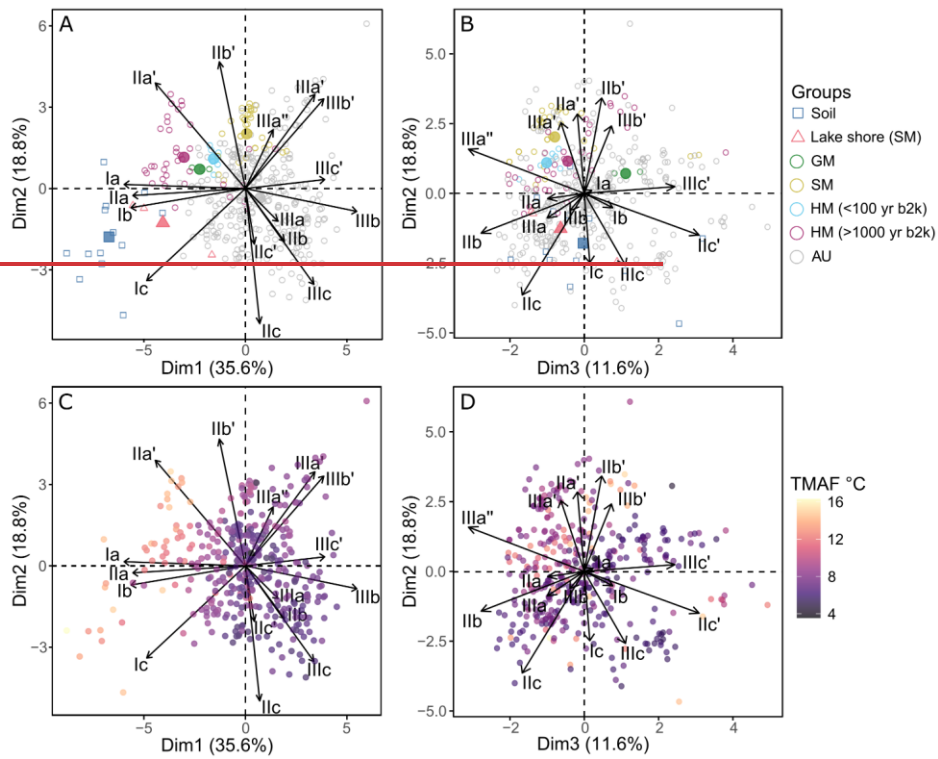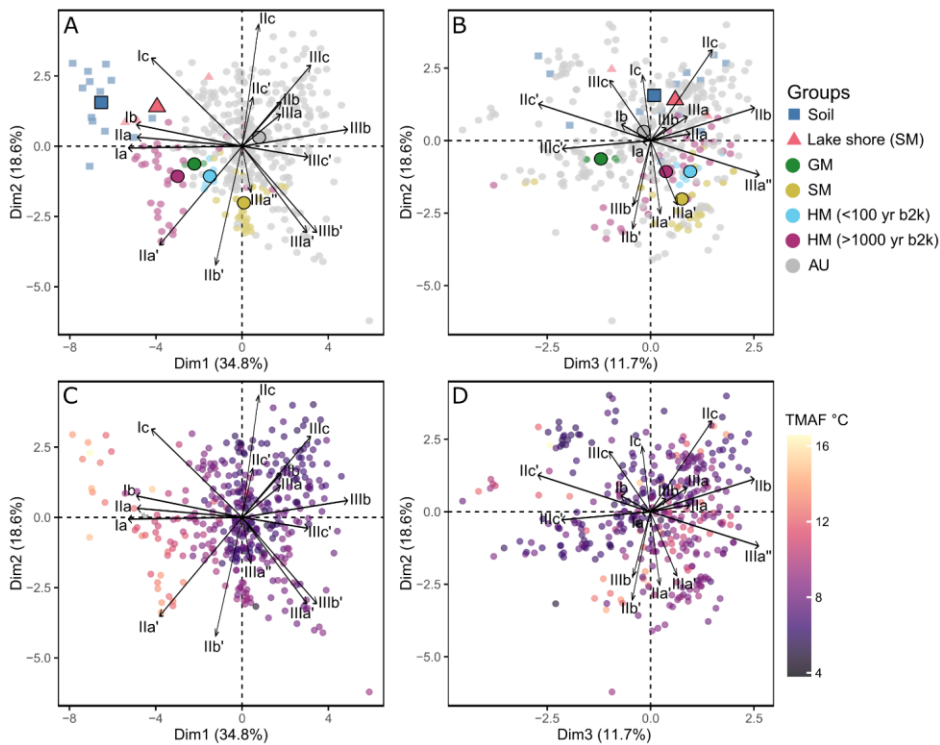
Figure 3: Principal component analysis biplots. Panels A and C show principal components 1 and 2. Panels B and D show principal components 2 and 3. Filled symbols in A and B represent the centroids of the groups (site or sample type). Fill in panels C and D is Raberg21_adj temperatures.

The test of calibration models reveals significant differences in GDGT-estimated temperatures (Figure 5~~Figure 5~~a). The soil models underestimate modern temperatures, which is to be expected when applied to lake sediments; however, three of the four soil calibrations also underestimate modern temperatures for the soil samples. The FROG$_0$ model produces temperature estimates with low errors, but also low variability. The two calibrations derived from African lakes (Russell et al., 2018) overestimate modern temperatures for all sample types, likely due to the fact that these models are calibrated for MAAT (mean annual air temperature) and are not well-suited for temperate lakes that are seasonally ice covered. The two recent global lake calibrations (Raberg et al., 2021; Martínez-Sosa et al., 2021) tend to underestimate modern temperatures for most of the lake sediment samples. Across all calibration models a consistent relationship can be observed between fIIIa'' and the offset between the GDGT-based temperature estimate and the modern instrumental temperature, with high values of fIIIa''

250 corresponding to a cold bias (Figure 5Figure 5a). High fIIIa'' is indicative of greater production of brGDGTs within the anoxic hypolimnetic waters of a stratified lake, which are substantially cooler than mixed surface layers, particularly in summer (Figure 4Figure 4). We note that oxygen is likely not the sole factor controlling IIIa'' production – nutrient levels and other biogeochemical parameters could influence fIIIa'' (Weber et al., 2018), but nonetheless it is a useful proxy for production of brGDGTs in the hypolimnion at these sites.

255
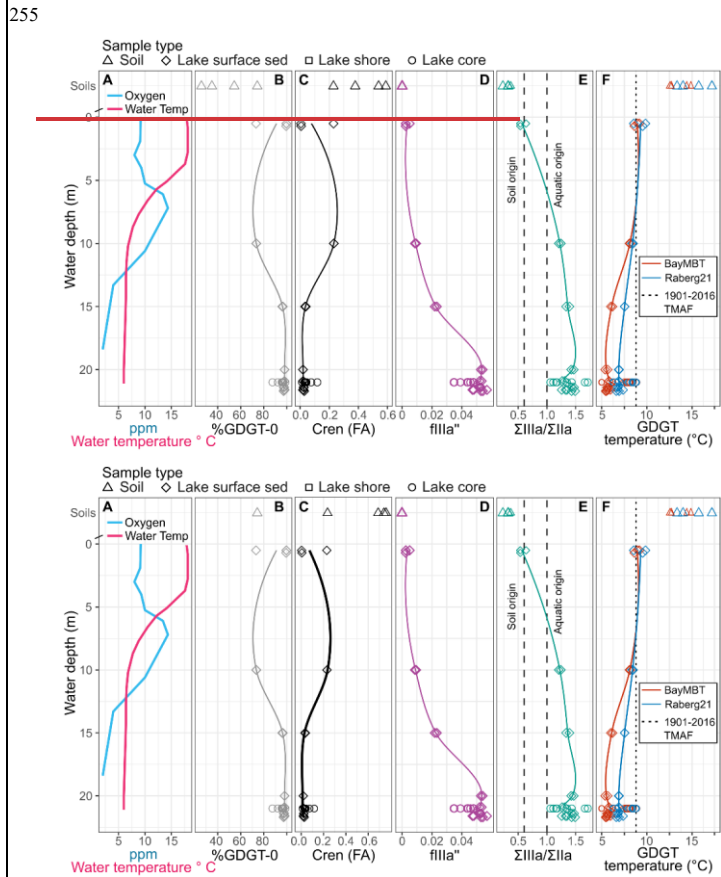
Figure 4: Depth transect at Schalkenmehrener Maar. A) Water temperature and oxygen concentration measured in water column in May 2007 (Sirocko, 2012). B-F) GDGT data from surface sediment samples taken along a depth transect. B) %GDGT-0 index showing relative abundance of methanogens and methanotrophs (Peaple et al., 2022; Sinninghe Damsté et al., 2012). C) Crenarchaeol fractional abundance of isoprenoid GDGTs indicating relative abundance of thaumarchaeota. D) Fractional abundance of IIIa''

260

relative to brGDGTs, indicating brGDGT production under anoxic conditions. E) ΣIIIa/ΣIIa ratio, a proxy for soil vs aquatic origin of brGDGTs. Thresholds for soil and aquatic origin from Xiao et al. (2016). F) brGDGT-inferred air temperatures (TMAF) from BayMBT (Martínez-Sosa et al., 2021) and Raberg21 (Raberg et al., 2021) calibrations.

265   Based on the observed inverse relationship between fIIIa'' and the temperature offsets, we calculated regression models to estimate the temperature bias associated with hypolimnetic production of brGDGTs for each calibration model. (Figure 5Figure 5b) shows the linear regression models for obtained by comparing the offsets of thethe BayMBT lake model and the Raberg21 model with fIIIa''. These regressions were found to be significant (p < 0.001), confirming our hypothesis that water-column stratification leads to a cold temperature bias in brGDGT temperature estimates. We utilize the regression models fit only to

270   lake sediment samples because the soil samples have temperature offsets that don't fit the linear trend and have distinct distributions from the lake samples. We then applied this correction to the temperature estimates from each calibration, which reduced the temperature offsets by accounting for the cold bias due to aquatic production of brGDGTs in bottom waters of the stratified maar lakes (Figure S1). Our data add to results from modern studies of brGDGTs at diverse lakes that have shown variable brGDGT composition along depth transects, suggesting that redox gradients could strongly influence brGDGT

275   composition (Van Bree et al., 2020; Weber et al., 2018, 2015; Stefanescu et al., 2021). We propose that the fIIIa'' correction should be tested at other sites and is likely useful to improve the accuracy of brGDGT temperature calibrations, particularly at lakes that experience prolonged stratification with extensive low oxygen zones.

Formatted: English (United States)

A) brGDGT Temperature Calibrations vs Modern

B) Example Correction Models

BayMBT Lake TMAF (Martínez-Sosa, 2021)

$y = 2.55 - 119\,x \quad R^2 = 0.73$
$y = 0.455 - 69.8\,x \quad R^2 = 0.59$

Lake TMAF (Raberg, 2021)

$y = 3.70 - 123\,x \quad R^2 = 0.66$
$y = 0.654 - 51.4\,x \quad R^2 = 0.62$
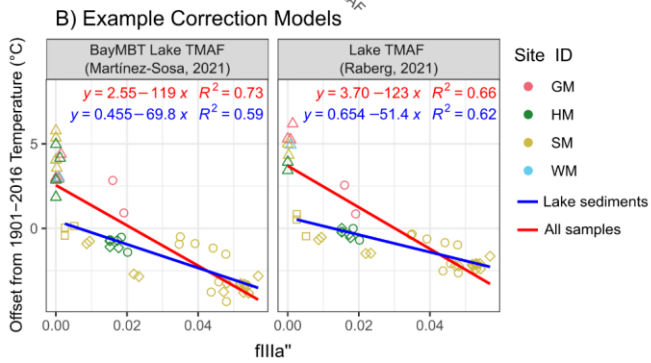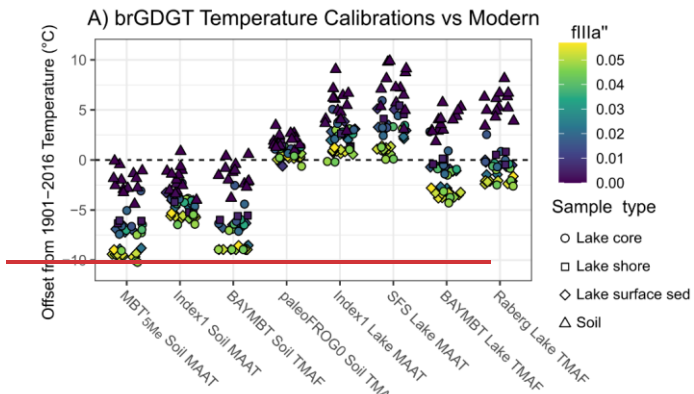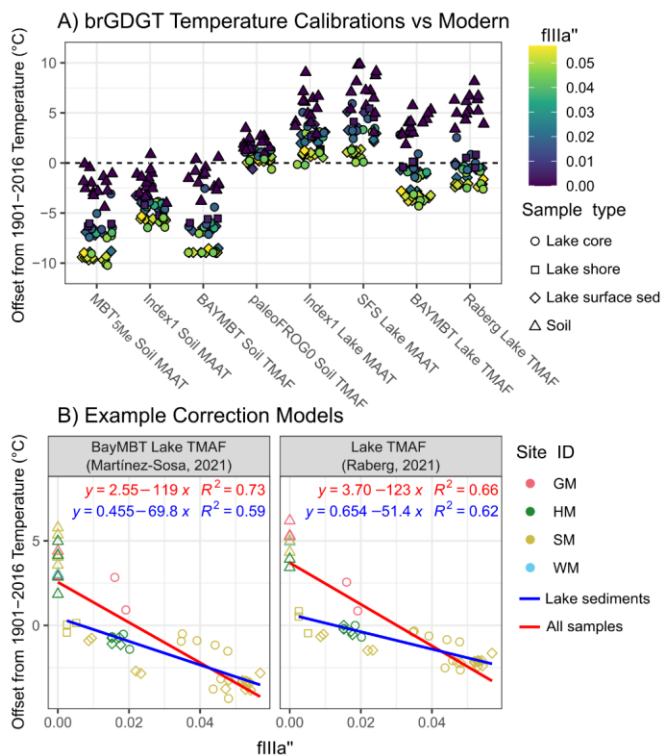
Figure 5: A) Offsets between brGDGT-inferred temperatures and 1901-2016 temperature data for eight different calibration models. Symbol shape corresponds to sample type, symbol fill corresponds to the fractional abundance of the IIIa'' isomer. B) Crossplots of temperature offsets and fIIIa'' for the two most recent lacustrine brGDGT temperature calibrations (Martínez-Sosa et al., 2021; Raberg et al., 2021). The regression model fit to lake samples (blue line) was used to correct the temperature reconstructions.

3.2 Assessing the impact of variable brGDGT sources on temperature reconstructions

We reconstructed TMAF using both the BayMBT and Raberg21 model, with and without the adjustment for cold bias associated with lake stratification and IIIa'' (Figure 6~~Figure 6~~). In this section, we interrogate the different reconstructions to understand if changing sources of brGDGTs may have biased the reconstructions:, in particular we assess evidence for variable contributions of brGDGTs from soils, epilimnetic production (warmer surface waters), and hypolimnetic production (cooler bottom waters). All four reconstructions show broadly similar multimillennial scale patterns, with mild temperatures near or slightly cooler than present during early MIS 3, a colder period from 35-25 kyr b2k with temperatures around 2-3 °C cooler

than present, and very warm temperatures during the mid-Holocene (2-5 °C warmer than present). The magnitude of LGM to Holocene warming is comparable across calibration models. However, significant differences occur during millennial-scale climate perturbations. The BayMBT model shows several periods of pronounced cooling that are, counterintuitively, synchronous with interstadials recorded in Greenland ice cores (GIs 3, 4, 5, 6, 9, 10, 11 in particular). These interstadial periods are associated with proxy evidence for greater oxygen depletion in the hypolimnion (increased C_{org}, S/Ti, and fIIIa''; Figure 7Figure 7); The adjusted BayMBT model shows a reduced magnitude of these cooling events, but nonetheless the contradictory cold interstadials remain. The Raberg21 model shows little change (cooling or warming) across these interstadial periods. This suggests that the BayMBT model is particularly sensitive to changes in brGDGT source, in particular the cold bias associated with increased production of brGDGTs in anoxic conditions. We interpret proxy evidence for increased primary productivity in the lake during interstadials to reflect a longer growing season. Furthermore, lake mixing likely also decreased either due to thermal stratification or a reduction of winds, leading to an expanded anoxic zone, and leading to a cold bias in the MBT'$_{5Me}$ proxy.

We tested the correlation of each of the four reconstructions with prominent temperature records from the last glacial period: δ^{15}N-based temperature estimates from Greenland ice cores (Kindler et al., 2014; Kobashi et al., 2017), alkenone-based sea surface temperatures (SST) from the Iberian margin (Martrat et al., 2007), and δD-based temperature estimates from the EPICA ice core in Antarctica (Jouzel et al., 2007). Correlations were calculated with each timeseries averaged into bins of three different widths: 250, 500, and 1000 years (Table 2Table 2). The Raberg21 models correlate more strongly with each of the tested paleoclimate records compared to the BayMBT models. Focusing on the Greenland temperature record and highest resolution binning, the Raberg21_adj has a Pearson correlation coefficient r = 0.71, while for BayMBT_adj r = 0.54. In particular, tThe BayMBT model shows particularly weak correlations if the period is restricted to 15-59 kyr b2k (r < 0.12 for all comparisons). The Raberg21 training data includes 43 sites from high-latitude environments that are not included in the BayMBT, and this may help improve the calibration for cold environments such as central Europe during the last glacial. The Raberg21_adj reconstruction shows higher correlations in all tests, and the correlations are significant (r > 0.70, p_adj < 0.05) for all comparisons for the full period (0-59 kyr b2k). If the correlation test is restricted to the period prior to the deglaciation (15-59 kyr b2k), correlations decrease, but the Raberg21_adj model remains significantly correlated with the Greenland temperature data. The significant correlations indicate that the Raberg21_adj model is a valid temperature reconstruction that captures the major climatic fluctuations of the past 60,000 years, and that the fIIIa'' correction method improves the accuracy of the reconstruction.
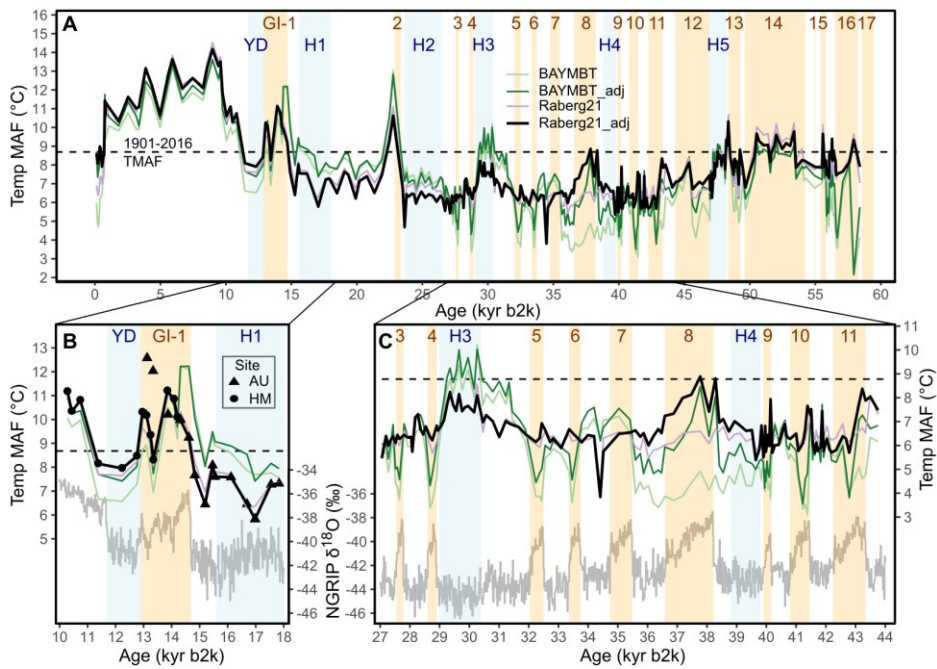
Figure 6: Comparison of brGDGT temperature reconstructions with and without correction for anoxic production of brGDGTs. Close-up panels show comparison with Dansgaard-Oeschger events in NGRIP ice core (gray, Rasmussen et al., 2014). Colored bars indicate Younger Dryas (YD), Greenland interstadials (GI) and Heinrich events (H).
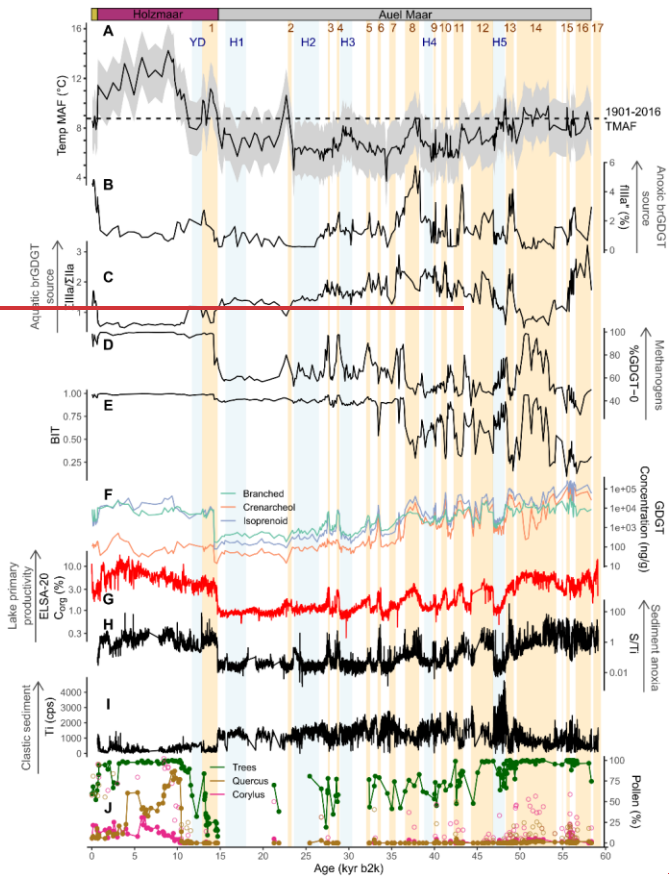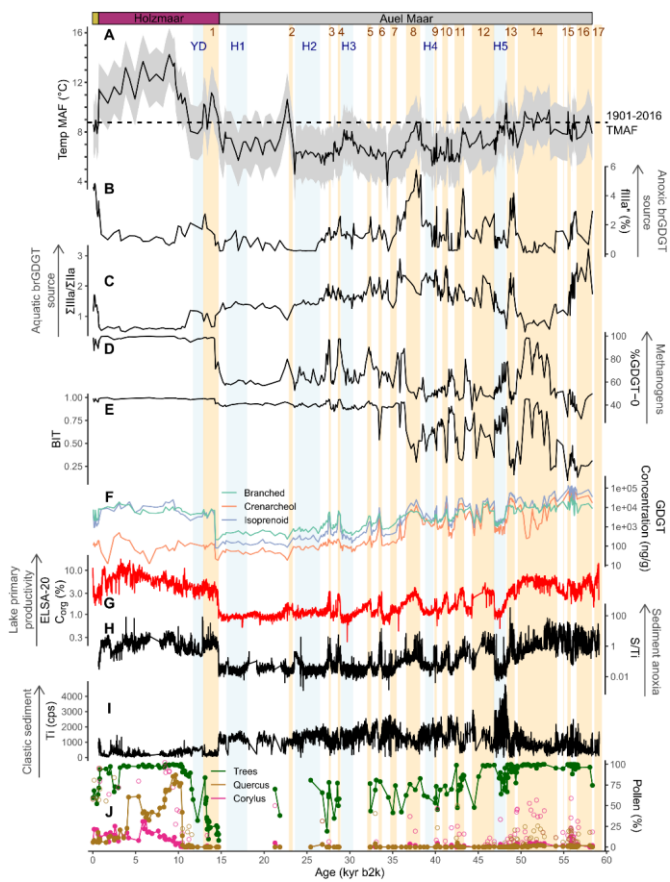
Figure 7: Proxy data from ELSA sediments. A) brGDGT temperature reconstruction (Raberg21_adj), gray shading indicates calibration uncertainty from Raberg et al. (2021). **B)** Fractional abundance of IIIa'' isomer indicating anoxic production of brGDGTs. **C)** ΣIIIa/ΣIIa ratio, a proxy for soil vs aquatic origin of brGDGTs. **D)** %GDGT-0 index showing relative abundance of methanogens and methanotrophs. **E)** BIT index showing relative proportion of brGDGTs to Crenarcheol. **F)** Concentrations of brGDGTs, isoprenoid GDGTs and crenarchaeol (including crenarchaeol isomer). **G)** C_{org} inferred from sediment reflectance (Sirocko et al., 2021). **H)** S/Ti ratio from XRF core scanning, used as a proxy for sediment/bottom-water anoxia. **I)** Ti counts, used as an indicator of lithogenic input. **J)** Tree pollen data with thermophilous species *Quercus* and *Corylus* highlighted (Sirocko et al., 2022). Non-filled circles in pollen plot represent 10x exaggerated pollen percentages.

335

Table 2: Correlation (~~Spearman's~~ Pearson ~~ρ~~r) between brGDGT temperature reconstructions and paleoclimate timeseries. Bold values indicated p < 0.05. P-values were adjusted for autocorrelation of the timeseries using the effective-n method (Dawdy and Matalas, 1964) and for multiple hypothesis testing using the false discovery rate method (Benjamini and Hochberg, 1995). Greenland temperatures from Kindler et al. (2014) and Kobashi et al. (2017). North Atlantic SST from alkenone $U^{K'}_{37}$ on core MD01-2444 (Martrat et al., 2007). Antarctica temperatures from δD measured on EPICA core (Jouzel et al., 2007).

	0-59 kyr b2k			15-59 kyr b2k		
	Greenland Temp	N. Atlantic SST	EPICA Temp	Greenland Temp	N. Atlantic SST	EPICA Temp
250-year bins						
Raberg21	**0.63**	**0.66**	**0.59**	0.27	**0.35**	0.32
Raberg21_adj	**0.71**	**0.70**	**0.70**	**0.39**	**0.42**	**0.48**
BayMBT	**0.47**	0.46	0.36	0.02	0.04	-0.01
BayMBT_adj	**0.54**	**0.51**	**0.46**	0.10	0.06	0.06
500-year bins						
Raberg21	**0.64**	**0.68**	0.59	0.29	0.38	0.25
Raberg21_adj	**0.71**	**0.72**	**0.71**	**0.43**	0.42	0.43
BayMBT	**0.47**	**0.48**	0.36	0.02	0.04	-0.08
BayMBT_adj	**0.54**	**0.52**	0.45	0.08	0.02	-0.01
1000-year bins						
Raberg21	**0.72**	**0.68**	0.60	0.42	0.34	0.24
Raberg21_adj	**0.77**	**0.72**	**0.71**	**0.53**	0.44	0.44
BayMBT	0.50	0.46	0.35	0.07	-0.01	-0.12
BayMBT_adj	**0.59**	**0.54**	0.45	0.12	0.01	-0.04

To further investigate what factors might influence mismatches between the GDGT temperature reconstructions and the Greenland temperature record, we calculated the offset between our four reconstructions and the Greenland temperatures after scaling the Greenland temperatures to match the mean and variance of the GDGT temperature estimates. These offsets were then correlated with paleoclimate and local proxy data (Figure 8~~Figure 8~~). This analysis shows that the offsets with Greenland temperatures tend to be negatively correlated with the paleoclimate records, indicating that our reconstructions tend to have a cold bias during warm periods (and/or vice versa). However, this relationship is substantially weaker for the Raberg21 models compared to the BayMBT model. The BayMBT models show strong negative correlations with C_{org} and fIIIa'', both of which are associated with greater aquatic production and hypolimnetic anoxia ~~weber~~ (Weber et al., 2018). The Raberg21 models also show negative correlations to these proxies, but the correlations are weaker, indicating the model is less sensitive to these non-climatic factors. The Raberg21_adj model is the only reconstruction that does not show a significant negative correlation between the offsets and fIIIa'', indicating that the cold bias associated with stratification has been mitigated due to the correction applied.

355
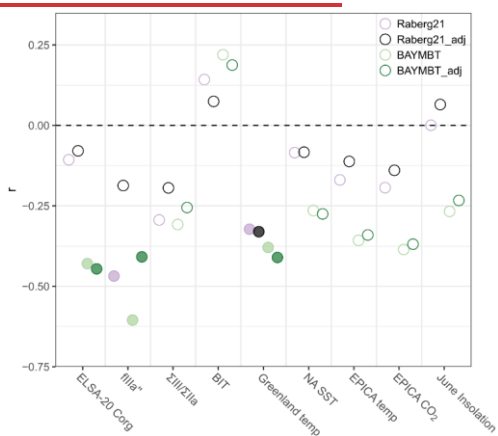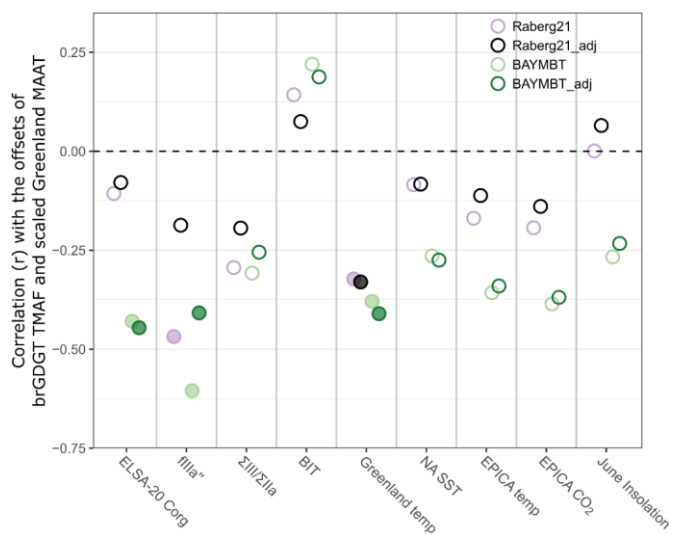
Figure 8: Assessing which factors contribute to offsets between GDGT temperature reconstructions and the Greenland δ¹⁵N temperature record after scaling mean and variance to match the GDGT temperatures (Kobashi et al., 2017; Kindler et al., 2014). Plotted is the Pearson's r for these offsets and the proxy timeseries on the x-axis. Timeseries were placed in 250-year bins before the correlation was calculated. Filled circles indicate significant correlations (p < 0.05 after adjusting for autocorrelation and multiple hypothesis testing).

360

Variations in aquatic vs soil sources of brGDGTs might influence the temperature reconstruction, as has been reported at other European lakes (Martin et al., 2019, 2020; Ramos-Román et al., 2022). No lake samples in this study are classified as soil samples by a machine learning algorithm that uses GDGT distributions to predict depositional environments (Martínez-Sosa et al., 2023), suggesting lacustrine sources dominate our lake sediment samples. CCorrelations between the Greenland

365 temperature offsets and ΣIIIa/ΣIIa and BIT could suggest that more (less) soil input is related to positive (negative) offsetstemperature overestimation. However, the correlations are not statistically significant, indicating that changing contribution of terrestrial vs aquatic sourced GDGTs is not a significant influence on the mismatch between the GDGT record and the Greenland record. Furthermore, although these two indices have been used in previous studies as indicators of soil derived GDGTs, global compilations provide mixed evidence of their utility. High BIT has been used as an indicator of

370 terrestrial GDGT sources (Hopmans et al., 2004), but in a global compilation of GDGT data (Martínez-Sosa et al., 2023), lake sediments actually have a higher average BIT than soils (p < 0.05). BIT is more likely to be controlled by the niche for crenarchaeol producing *Thaumarchaeota.* The interpretation of low ΣIIIa/ΣIIa as indicative of soil derived brGDGTs was originally proposed for marine settings (Xiao et al., 2016), but has also been applied to lacustrine GDGTs (Martin et al., 2020). However, 65% of lake sediment samples in a global compilation (Raberg et al., 2022) have ΣIIIa/ΣIIa < 1, suggesting that

375 calibration models for lacustrine sediments already account for some degree of soil input, or ΣIIIa/ΣIIa < 1 is commonly produced in lacustrine environments. Additionally, the ΣIIIa/ΣIIa ratio is strongly negatively correlated with temperature in global compilations of lacustrine brGDGTs (Raberg et al., 2022), in particular at for values < 1. Thus fluctuations in ΣIIIa/ΣIIa may be driven by temperature change rather than variable portions of aquatic vs terrestrial brGDGTs. Alternatively, because ΣIIIa/ΣIIa changes with depth in our SM transect (Figure 4), this index may be influenced by variable biogeochemical

380 conditions that control the niches of IIa vs IIIa producers, similar to IIIa''. An additional point of evidence that soil sources do not dominate the GDGT distribution is that no lake samples are identified as soil samples by a machine learning algorithm that uses GDGT distributions to predict depositional environments (Martínez-Sosa et al., 2023).

In our 60,000-year reconstruction, low ΣIIIa/ΣIIa and high BIT mainly occur during the interval represented by Holzmaar

385 sediments. The composition of GDGTs in HM is unique in that it has low concentrations of Crenarchaeol, specifically produced by ammonium oxidizing *Thaumarchaeota*, and high GDGT-0, produced by methanogens. These characteristics indicate that isoprenoid GDGTs have an aquatic (anoxic) source in HM. C/N ratios in organic matter in HM sediments are typically 9-11, also indicating a dominantly aquatic source for organics in HM (Anhäuser et al., 2014; Lücke et al., 2003). HM sediments plot between lake and soil samples from the Eifel in reduced dimensional space (Figure 3Figure 3), however the similarity with

390 soil is mainly driven by the first principle component, which is highly correlated to temperature, and therefore it is unclear if the similar composition of HM and soils could be due to HM representing the warmest period in the record (Holocene Thermal Maximum; Kaufman and Broadman, 2023). PCs 2 and 3 show distinct differences between HM and soil samples. When compared to a global compilation of GDGTs (Martínez-Sosa et al., 2023), HM plots outside the range of soil samples in a PCA (Figure S2). Overall, there is evidence that HM GDGTs differ from the other sites with some evidence for a greater

395 portion of soil-derived brGDGTs; however, there is also evidence that the GDGTs are still predominantly aquatic. The distinct composition of HM GDGTs could be related to a steep ~~oxycline~~ redox gradient and extensive euxinic conditions in HM, as indicated by the presence of pigments attributed to anoxygenic phototrophic bacteria in Holocene sediments of HM (S. Birlo, G. Wienhues, personal communication). The same pigments were not detected in sediments from Auel Maar ~~(P. Zander, unpublished~~(Albert et al., In review)~~)~~. The euxinic conditions in HM ~~likely~~ restrict the abundance of *Thaumarchaeota* (Callieri

400 et al., 2016; Sinninghe Damsté et al., 2022), driving low BIT values. brGDGT production in the anoxic zone was apparently relatively low (low fIIIa'') in Holocene HM, and this points toward a greater proportion of brGDGTs produced in the warm epilimnion of HM or in catchment soils, which could be a justification for anomalously warm temperatures in the HM segment. Similarity of the HM Holocene samples and SM lake shore samples (<1 m water depth) strengthen this interpretation (Figure 3~~Figure 3~~, Figure 4~~Figure 4~~). The reasonable agreement (considering significant age uncertainty in the Auel Maar data) of

405 reconstructed temperature from samples taken from both Auel Maar and Holzmaar during the Bolling-Allerod warm period (GI-1) is evidence that compatible results can be obtained from both sites despite substantially different sediment properties in this interval (Figure 6~~Figure 6~~).

Modelled TMAF from a high-resolution global circulation model (HadCM3; (Leonardi et al., 2023; Beyer et al., 2020) agrees

410 with brGDGT-inferred temperatures (Figure 9~~Figure 9~~), though the model is not capable of capturing millennial-scale variations. The root mean square deviation between proxy and model is 2.19 °C, nearly identical to the calibration error of 2.14 °C. The Holocene segment from Holzmaar is the only prolonged period of deviation between the model and proxy data, which ~~may~~ might be attributed to changing brGDGT sources as described above. However, it is likely that the model output also underestimates TMAF to some extent during the Holocene thermal maximum (HTM; 5-11 kyr BP) due to an

415 underestimation of vegetation expansion and subsequent albedo feedbacks during the HTM (Thompson et al., 2022). Proxy data from Europe consistently show warmer than present summer temperatures during the HTM (Kaufman and Broadman, 2023; Martin et al., 2020; Renssen et al., 2009; Kaufman et al., 2020), which is not observed in the model output.
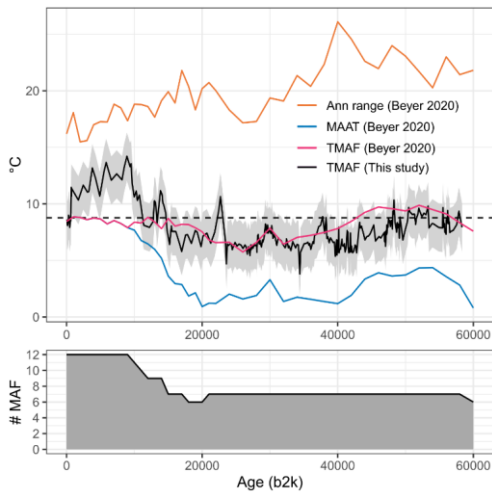
Figure 9: Comparison of HadCM3 model simulations (Beyer et al., 2020; Leonardi et al., 2023) of seasonality, MAAT and TMAF with brGDGT temperature reconstruction.

3.3 Comparison with regional paleoclimate records

The TMAF reconstruction shows multi-millennial patterns and magnitudes of change that are congruent with existing temperature reconstructions from Europe (Figure 10~~Figure 10~~). An early MIS-3 warm period occurs from 54-51 kyr b2k (GI-14) in which TMAF is approximately the same as modern conditions (9 °C). This warm period corresponds with the ~~prescence~~presence of thermophilous tree species *Quercus* and *Corylus* in the study area ~~(Figure 7Fi~~(Sirocko et al., 2022)~~gure 7)~~, as well as an interval of speleothem growth in central European caves, a qualitative indicator of warm conditions (Riechelmann et al., 2023). Evidence of summer temperatures near modern levels during early MIS-3 can also be found from insect remains in N. Finland, the British Isles and France (Helmens, 2014) and peak temperatures recorded in an Austrian speleothem (Spötl and Mangini, 2002). During Heinrich event 5 (H5), brGDGTs record relatively warm temperatures in contrast to severely depressed SST in the North Atlantic at this time (Figure 10~~Figure 10~~; Martrat et al., 2007). Low ΣIIIa/ΣIIa, low C_{org}, and high Ti could indicate a shift towards more soil-derived brGDGTs during H5 (Figure 7~~Figure 7~~), which would lead to a warm bias in the TMAF reconstruction. Alternatively, enhanced seasonality may have led to higher TMAF despite cold long winters (Denton et al., 2022). Following H5, temperatures enter a cool phase from 44-38 kyr b2k, corresponding with a minimum of summer insolation, and including H4. GI-8 stands out as prolonged warm period in our record, with ~2 °C of warming at the onset of the interstadial. After gradual cooling, TMAF averages 6.4 °C from 36-30.5 kyr b2k. HE3 is again associated with an increase in TMAF, most likely associated with a prolonged freezing-season.
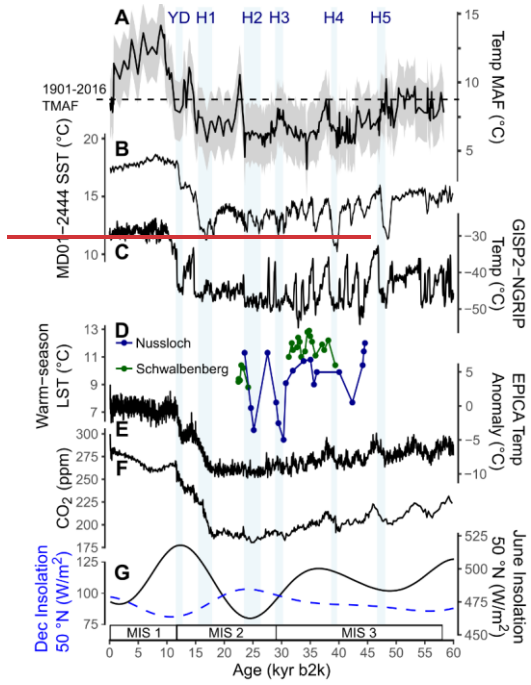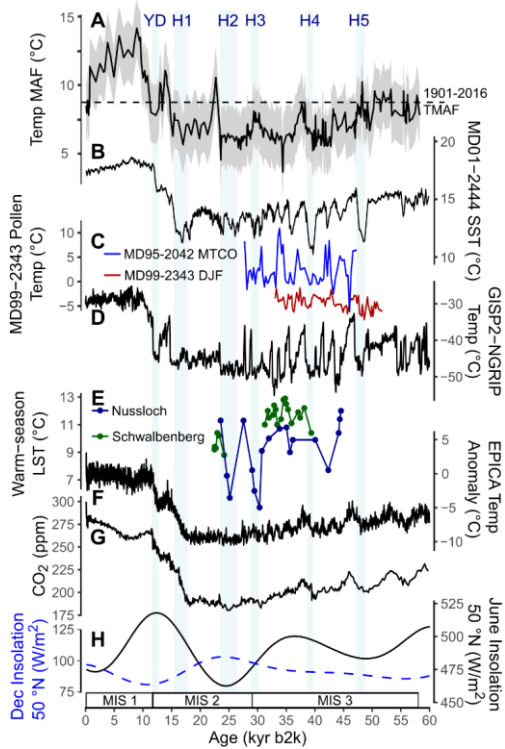
Figure 10: Comparison of ELSA brGDGT temperature reconstruction with regional and global paleoclimate records. **A)** brGDGT temperature reconstruction (Raberg21_adj). **B)** North Atlantic SST from core MD01-2444 based on alkenone U$^{k'}_{37}$ proxy (Martrat et al., 2007). C) Pollen-based temperature reconstructions from the SW coast of the Iberian peninsula (MD95-2042; (Sánchez Goñi et al., 2002) and northwest Mediterranean Sea (MD99-2343; (Sánchez Goñi et al., 2021). MTCO = mean temperature of coldest month; DJF = December, January, and February mean temperature. ~~D~~C) Greenland $\delta^{15}N$ temperatures (Kobashi et al., 2017; Kindler et al., 2014). ~~D~~E) Earthworm calcite grain warm season land surface temperatures (LST) from German loess (Prud'homme et al., 2022). ~~F~~E) Antarctica temperature anomalies from δD (Jouzel et al., 2007). ~~G~~F) Atmospheric CO_2 estimated from the EPICA ice core (Bereiter et al., 2015). ~~H~~E) Incoming solar insolation for 50 °N during summer (black line) and winter (blue dashed line) (Laskar et al., 2004).

From 29-24 kyr b2k TMAF reaches lowest levels of the record (~6.2 °C), in good agreement with the timing of maximal glacier extent in the Alps (Seguinot et al., 2018), British Isles and Baltic lowlands (Clark et al., 2009). The estimate of 2.6 °C cooling during the LGM compared to modern is substantially less than noble gas estimates of -9.1 °C LGM cooling from the Paris Basin at 26 kyr BP (Bekaert et al., 2023) and the results of a global paleoclimate data assimilation (~10 °C cooling at our site for 23-19 kyr BP; Tierney et al., 2020). However, considering the stronger seasonal variability during the LGM, and thus

longer freezing period, changes in TMAF are expected to be smaller than MAAT. Beetle (Coleoptera) remains from Auel Maar indicate that during the LGM, temperatures of the warmest month were 6 to 9.5 °C, whereas temperatures of the coldest month were -20 to -30 °C (Britzius and Sirocko, 2022), approximately double the annual temperature range compared to modern. Scaling the modern monthly climatology to match these temperatures would yield a TMAF between 5.8 and 4.3 ° C, which overlaps with our estimated 4.0-8.3 °C, taking into account calibration uncertainty (Figure 11Figure 11). HadCM3 model output yields an TMAF of 6.3 °C over the 24-29 kyr period, nearly identical to the brGDGT estimate (Leonardi et al., 2023; Beyer et al., 2020). In the model output, the number of months above freezing was 6-7 months during MIS 2-3 with an amplified seasonal temperature range of mean monthly temperature up to 26 °C (modern range is 16°C) (Figure 9Figure 9). The enhanced seasonal range helps to explain the much smaller TMAF cooling compared to MAAT (Figure 11Figure 11).
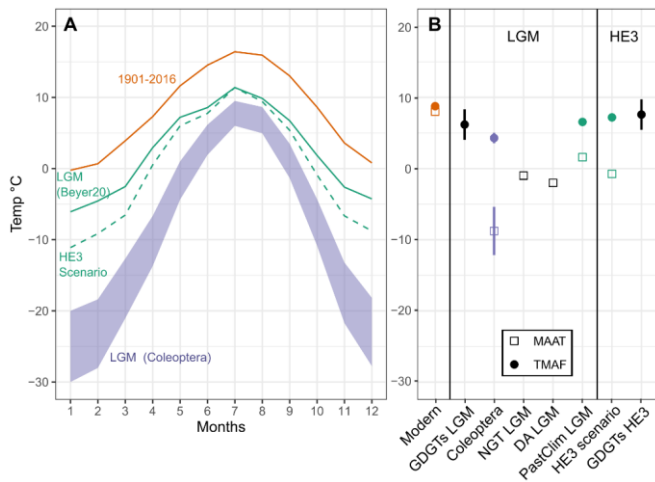
Figure 11: A) Comparison of modern seasonal temperature range for the modern period, LGM based on climate models (Beyer et al., 2020), LGM based on Coleoptera remains (Britzius and Sirocko, 2022), and a hypothetical Heinrich event scenario in which winter temperatures decrease while peak summer temperatures remain the same. B) Comparison of TMAF and MAAT for modern, LGM and HE3 based on different methods. NGT LGM = Noble Gas Temperatures from (Bekaert et al., 2023), DA LGM = data assimilation results from (Tierney et al., 2020). Notes: Coleoptera temperature range was obtained by scaling modern monthly temperatures to match the Coleoptera estimates of warmest and coldest months, the ranges represent likely values based on a simple assumption about the monthly temperature pattern, but are not a calibrated estimate.

Two ~~data points~~samples suggest anomalously high TMAF near modern values during GI-2 (the ages of these samples are slightly younger than GI-2, but we attribute them to GI-2), which are suggestive of seasonally warm temperatures, though additional data would be needed to confidently confirm this interpretation. The pattern of deglacial warming captures major features such as the Bolling-Allerod warm period, Younger Dryas stadial, and rapid warming during the early Holocene. The Bølling–Allerød (GI-1) TMAF is slightly warmer than modern and 2.8 °C warmer than H1. Chironomid-based summer

temperature reconstructions from the alpine region and NW Europe suggest broadly similar magnitudes of warming from H1 to GI-1 (Heiri et al., 2015, 2014). Low sampling resolution precludes meaningful estimates of Younger Dryas cooling. Mid-Holocene temperatures average 12.3 °C, or 3.5 °C warmer than present, suggestive of a strong Holocene thermal maximum combined with strong seasonality in response to high summer insolation. The magnitude of the HTM is greater than estimated from pollen-based summer temperature reconstructions (Mauri et al., 2015; Renssen et al., 2009; Martin et al., 2020), but is similar to the magnitude of warming in chironomid-based reconstructions from the alpine region (Heiri et al., 2015).

3.4 Minimal millennial-scale variability in summer temperatures during the last glacial period

Our GDGT temperature reconstruction shows substantially dampened millennial-scale climate variability in comparison with paleoclimate records from the North Atlantic region.

Table 3 shows the temperature and warming estimated for each Greenland Interstadial (GI) and the early Holocene. For all but one GI from 59-24 ky b2k (GIs 3-16), the warming is less than 1 ° C, which is less than the error of the temperature calibration (2.14 °C). We calculate a mean warming of 0.5 +/- 1.3 °C for GIs 1-16, significantly less than observed in Greenland (average = 5.5 °C). These results suggest that Dansgaard-Oeschger (DO) cycles had a minimal impact on warm-season temperatures in central Europe. This finding is surprising considering major changes observed in aquatic productivity and redox conditions in Auel Maar and other lakes in western Europe (Wohlfarth et al., 2008) during DODO cycles. Additionally, pollen records indicate major vegetation shifts associated with DODO cycles (Wohlfarth et al., 2008; Moreno et al., 2014; Duprat-Oualid et al., 2017; Guiot et al., 1993; Sánchez Goñi et al., 2008), and shifts in $\delta^{18}O$ (Spötl and Mangini, 2002; Moseley et al., 2014) and $\delta^{13}C$ (Genty et al., 2003) measured on speleothems indicate major changes to atmospheric circulation and terrestrial ecosystems, respectively. However, our record supports the hypothesis that these changes were driven primarily by variability in winter temperatures associated with expanded sea ice (Denton et al., 2005, 2022; Flückiger et al., 2008). Changes in the duration of the growing season likely had a major impact on biotic proxies such as pollen and lake productivity.

Quantitative estimates of millennial-scale temperature fluctuations from terrestrial archives in Europe are rare beyond the past 15 kyr. Additionally, estimates of seasonal temperatures are challenging to interpret due to the difficulty of disentangling multiple climate signals. Isotopic measurements of earthworm calcite granules from the Rhine Valley, Germany were used to estimate approximately 1-4 °C of warming during the warmest monthswarmer land surface temperatures during during warm seasons during GIs-interstadials compared to stadials (Prud'homme et al., 2022). Clumped isotope measurements on snails in Hungary indicate a difference of 4-7 °C between stadial and interstadial phases for the growing season (Újvári et al., 2021). Temperatures estimated from diatom assemblages at Les Echets, France suggest 0.5-2 °C of summer warming during GIs between 18-36 kyr BP (Ampel et al., 2010). Pollen assemblages from marine sediments on the Iberian margin and in the Mediterranean suggest that winter (DJF) temperatures in the Iberian peninsula and southern France decreased by approximately 1.5-2.5 °C during Heinrich events 4 and 5 (Sánchez Goñi et al., 2021). The mean temperature of the coldest month in Iberia was estimated to be approximately similar to modern day during interstadials of the last glacial, but cooled by

as much as 8 °C during HE4 (Sánchez Goñi et al., 2002). (Sánchez Goñi et al., 2002, 2021, 2008)Moraine records from Alpine glaciers provide evidence of lowof muted millennial-scale summer temperature variability in Europe; simulations of Alpine ice extent fit the moraine records better when forced by temperatures scaled to the Antarctica temperature record, rather than Greenland (Seguinot et al., 2018). Model simulations of DODO type variability also provide variable results. Two simulations done with LOVECLIM using perturbations in Atlantic meridional overturning circulation (AMOC) yielded very different estimates for DODO cycle temperature variability. Using the LOVECLIM model, Van Meerbeeck et al. (2011), estimated 8 °C warming in Europe during the warmest month and 17 °C warming during the coldest month for a stadial-interstadial transition during early MIS-3, whereas Menviel et al. (2020) report 1.5 °C warming of MAAT over Europe associated with stadial-interstadial changes at 37 kyr BP, also using LOVECLIM. A modeling study that isolated the impact of AMOC changes showed that, in Europe, spring temperatures changed more than any other season in response to a shift from weak to strong AMOC, with 3.5 °C of warming in spring compared 2 °C in summer (Flückiger et al., 2008). The variations in spring temperatures would have important implications for the brGDGT proxy by changing the length of the non-freezing season.

Table 3: Temperatures of warm events recorded by ELSA GDGT reconstruction and compared to temperature changes recorded in Greenland.

Time period	Start (yr b2k)	End (yr b2k)	GDGT TMAF (°C)	n (interstadial)	Warming from previous stadial (°C)	n (stadial)	Greenland Temp (°C)	Greenland warming (°C)
Early Holocene	11700	8326	11.70	10	3.53	2	-28.86	15.16
GI-1	14692	12896	9.91	9	2.83	17	-37.97	7.35
GI-2	23340	22400	9.97	2	3.82	25	-44.66	3.19
GI-3	27780	27540	6.34	2	-0.23	10	-41.24	7.12
GI-4	28900	28600	6.27	2	-0.95	23	-40.40	7.41
GI-5	32500	32040	6.44	3	0.22	4	-44.24	7.07
GI-6	33740	33360	6.59	2	0.91	5	-45.42	3.82
GI-7	35480	34740	6.50	2	0.07	7	-40.41	6.73
GI-8	38220	36580	7.82	6	1.05	11	-40.83	6.81
GI-9	40160	39900	6.27	8	0.04	7	-45.75	1.75
GI-10	41460	40800	6.48	6	0.21	16	-41.15	6.10
GI-11	43340	42240	6.70	9	-0.75	5	-42.08	8.10
GI-12	46860	44280	7.20	7	-0.74	34	-39.37	6.49
GI-13	49280	48340	8.04	12	0.18	1	-42.07	0.71
GI-14	54220	49600	8.75	19	0.70	2	-40.36	5.95
GI-15	55800	55400	8.38	5	0.14	22	-40.48	6.07
GI-16	58280	56500	8.03	5	0.12	1	-41.56	4.50

The GDGT temperature reconstruction shows a variable response to North Atlantic Heinrich Events. H5 and H3 are associated with slight warmings in our reconstruction, and H1 has relatively mild temperatures. These results appear to be consistent with

major meltwater pulses recorded in sediments from the Bay of Biscay indicating melting of European ice sheets and glaciers during Heinrich Events 1-3 (Toucanne et al., 2015), which would require relatively warm summers. Denton et al. (2022) summarize existing evidence for relative warmth during Heinrich summers.

530 The seasonal response of lacustrine brGDGTs to the non-freezing season is a primary reason why our estimate of stadial-interstadial temperature variability is lower than other records from Europe. Over the instrumental period, TMAF and MAAT are nearly the same for our study area (8.77 °C vs 8.1 °C); however, during the last glacial period, with cooler temperatures and increased continentality, the difference between MAAT and TMAF would have increased substantially (Figure 9Figure 9). We demonstrate that it is possible for the combination of cooler MAAT and increased seasonality to increase TMAF by

535 simulating a hypothetical HE3 monthly temperature pattern which that has the July temperature simulated by HadCM3 for the LGM from Beyer et al. (2020), but with a 5 °C greater seasonal range, i.e., January temperatures are 5 °C colder (Figure 11Figure 11). 5 °C cooling is realistic for a Heinrich event based on a similar, or even greater range of variability in the mean temperature of coldest months (MTCO) during millennial-scale events in a pollen-based reconstruction from the Iberian Margin (Figure 10; Sánchez Goñi et al., 2002). Compared to the LGM values, this simulated Heinrich event would have

540 MAAT 2.6 °C cooler, but TMAF is 1.1 °C warmer. This assumes a constant shape of the annual temperature cycle; however, particularly cold spring temperatures during Heinrich events (Flückiger et al., 2008) could enhance this effect. This response to the changing duration of the non-freezing period dampens variability in brGDGT temperature reconstructions when colder temperatures are associated with increased seasonal amplitude, highlighting the importance of incorporating knowledge of the recording season of paleoclimate archives. when interpreting paleoclimate records (Kwiecien et al., 2021). Temperature

545 calibrations rely on an assumption that brGDGTs respond to TMAF, but detailed knowledge of seasonal production of brGDGTs might improve interpretation of temperature reconstructions, particularly because the organisms producing brGDGTs in lakes are not yet identified. Field monitoring studies of lacustrine brGDGT production suggests that production can be dominated by relatively short periods in the year and can be triggered by mixing events (Loomis et al., 2014; Van Bree et al., 2020), which could bias the temperature signal to record conditions associated with lake mixing (typically 4-8 ° C for

550 temperate lakes).

Overall, our data add to a growing body of evidence that changes in seasonality, and particularly winter climate, drove the abrupt millennial-scale climate events of the last glacial period, while summer temperatures remained relatively stable and moderate.

555 **4. Conclusions**

GDGT distributions measured on a composite sequence of lake sediments from the Eifel volcanic field, Germany provide a unique tool to reconstruct temperature fluctuations in central Europe during the past 60 kyr. A comparison of modern GDGT

distributions in soils and lakes from the Eifel provides insights into the accuracy of the various published brGDGT-temperature calibrations. We find that lake stratification likely leads to a cold bias in brGDGT temperature estimates, and that this bias can

560 be corrected for using the relationship between the residuals of the temperature calibrations in this region and the IIIa'' isomer, which is exclusively produced in anoxic conditions. We find that the multivariate calibration model of Raberg et al., 2021 performs best, and after adjusting for the effect of lake stratification, produces a temperature reconstruction that resembles other temperature reconstructions from the past 60 kyr. The adjusted Raberg21 model is less affected by non-climatic factors, such as changing sources of brGDGTs. A proxy-model comparison shows generally good agreement, and highlights the

565 important role of seasonality in the temperature recorded by brGDGTs. Our centennial-resolution reconstruction of TMAF indicates that early MIS-3 experienced non-freezing-season temperatures only slightly cooler than present, and that LGM TMAF was approximately 2.6 °C cooler than present. The TMAF reconstruction shows only minimal 0-1 °C temperature fluctuations across Greenland stadial-interstadial transitions, strong evidence that these millennial scale climate events primarily affect the winter season and shortened growing seasons, but peak warm-season temperatures were less affected. The

570 seasonal signal of TMAF provides a unique constraint on our understanding of past ~~seasonality~~ changes to seasonal temperature cycles and thus may be a useful target for modeling studies of past climate. Our high-resolution, continuous temperature reconstruction is unique for the European continent and therefore will be of interest for studies of paleoecology and archaeology.

575 *Author contributions.* PDZ: Conceptualization, Formal analysis, Investigation, Writing - original draft, Visualization; DB: Conceptualization, Formal analysis, Investigation; Writing – review & editing; FS: Conceptualization, Investigation, Resources, Funding acquisition, Project administration; Writing – review & editing; AA: Formal analysis, Writing – review & editing; GH: Resources, Funding acquisition, Project administration; AMG: Conceptualization, Resources, Funding acquisition, Project administration; Writing – review & editing.

580

Code and data availability. Data has been submitted to Pangaea, a DOI will be included in the published manuscript. Code ~~can be made available on request~~will be made available at https://github.com/PaulDZander/EifelGDGTs.

Competing interests. The authors declare no competing interests.

585

Acknowledgements. The work was funded by the University of Mainz, Germany, the Max Planck Institute for Chemistry, Germany, and the Swiss National Science Foundation grant # P500PN_206731. We thank Klaus Schwibus, Yvonne Hamann, Brigitte Stoll, and Mareike Schmitt for technical assistance.

References

Albert, J., Zander, P. D., Grosjean, M., and Sirocko, F.: Fine-tuning of sub-annual resolution spectral index time series 2 from Eifel maar sediments, Western Germany, to the NGRIP 3 δ18O chronology, 26–60 ka, Quaternary, In review.

Ampel, L., Bigler, C., Wohlfarth, B., Risberg, J., Lotter, A. F., and Veres, D.: Modest summer temperature variability during DO cycles in western Europe, Quaternary Science Reviews, 29, 1322–1327, https://doi.org/10.1016/j.quascirev.2010.03.002, 2010.

Anhäuser, T., Sirocko, F., Greule, M., Esper, J., and Keppler, F.: D/H ratios of methoxyl groups of the sedimentary organic matter of Lake Holzmaar (Eifel, Germany): A potential palaeoclimate/-hydrology proxy, Geochimica et Cosmochimica Acta, 142, 39–52, https://doi.org/10.1016/j.gca.2014.08.001, 2014.

Auderset, A., Schmitt, M., and Martínez-García, A.: Simultaneous extraction and chromatographic separation of n-alkanes and alkenones from glycerol dialkyl glycerol tetraethers via selective Accelerated Solvent Extraction, Organic Geochemistry, 143, 103979, https://doi.org/10.1016/j.orggeochem.2020.103979, 2020.

Bechtel, A., Smittenberg, R. H., Bernasconi, S. M., and Schubert, C. J.: Distribution of branched and isoprenoid tetraether lipids in an oligotrophic and a eutrophic Swiss lake: Insights into sources and GDGT-based proxies, Organic Geochemistry, 41, 822–832, https://doi.org/10.1016/j.orggeochem.2010.04.022, 2010.

Bekaert, D. V., Blard, P.-H., Raoult, Y., Pik, R., Kipfer, R., Seltzer, A. M., Legrain, E., and Marty, B.: Last glacial maximum cooling of 9 °C in continental Europe from a 40 kyr-long noble gas paleothermometry record, Quaternary Science Reviews, 310, 108123, https://doi.org/10.1016/j.quascirev.2023.108123, 2023.

Benjamini, Y. and Hochberg, Y.: Controlling the False Discovery Rate: A Practical and Powerful Approach to Multiple Testing, Journal of the Royal Statistical Society: Series B (Methodological), 57, 289–300, https://doi.org/10.1111/j.2517-6161.1995.tb02031.x, 1995.

Bereiter, B., Eggleston, S., Schmitt, J., Nehrbass-Ahles, C., Stocker, T. F., Fischer, H., Kipfstuhl, S., and Chappellaz, J.: Revision of the EPICA Dome C CO2 record from 800 to 600 kyr before present, Geophysical Research Letters, 42, 542–549, https://doi.org/10.1002/2014GL061957, 2015.

Beyer, R. M., Krapp, M., and Manica, A.: High-resolution terrestrial climate, bioclimate and vegetation for the last 120,000 years, Sci Data, 7, 236, https://doi.org/10.1038/s41597-020-0552-1, 2020.

Bohm, E., Lippold, J., Gutjahr, M., Frank, M., Blaser, P., Antz, B., Fohlmeister, J., Frank, N., Andersen, M. B., and Deininger, M.: Strong and deep Atlantic meridional overturning circulation during the last glacial cycle, Nature, 517, 73–76, https://doi.org/10.1038/nature14059, 2015.

Britzius, S. and Sirocko, F.: Subfossil Coleoptera from Eifel maar sediments as indicators of the environmental evolution in Central Europe over the last 60,000 years, Palaeogeography, Palaeoclimatology, Palaeoecology, 596, 110981, https://doi.org/10.1016/j.palaeo.2022.110981, 2022.

Brunck, H., Sirocko, F., and Albert, J.: The ELSA-Flood-Stack: A reconstruction from the laminated sediments of Eifel maar structures during the last 60 000 years, Global and Planetary Change, 142, 136–146, https://doi.org/10.1016/j.gloplacha.2015.12.003, 2016.

Callieri, C., Hernández-Avilés, S., Salcher, M. M., Fontaneto, D., and Bertoni, R.: Distribution patterns and environmental correlates of Thaumarchaeota abundance in six deep subalpine lakes, Aquat Sci, 78, 215–225, https://doi.org/10.1007/s00027-015-0418-3, 2016.

Cao, J., Rao, Z., Shi, F., and Jia, G.: Ice formation on lake surfaces in winter causes warm-season bias of lacustrine brGDGT temperature estimates, Biogeosciences, 17, 2521–2536, https://doi.org/10.5194/BG-17-2521-2020, 2020.

Chen, Y., Zheng, F., Yang, H., Yang, W., Wu, R., Liu, X., Liang, H., Chen, H., Pei, H., Zhang, C., Pancost, R. D., and Zeng, Z.: The production of diverse brGDGTs by an Acidobacterium providing a physiological basis for paleoclimate proxies, Geochimica et Cosmochimica Acta, https://doi.org/10.1016/j.gca.2022.08.033, 2022.

Clark, P. U., Dyke, A. S., Shakun, J. D., Carlson, A. E., Clark, J., Wohlfarth, B., Mitrovica, J. X., Hostetler, S. W., and McCabe, A. M.: The Last Glacial Maximum, Science, 325, 710–714, https://doi.org/10.1126/science.1172873, 2009.

Compo, G. P., Whitaker, J. S., Sardeshmukh, P. D., Matsui, N., Allan, R. J., Yin, X., Gleason, B. E., Vose, R. S., Rutledge, G., Bessemoulin, P., Brönnimann, S., Brunet, M., Crouthamel, R. I., Grant, A. N., Groisman, P. Y., Jones, P. D., Kruk, M. C., Kruger, A. C., Marshall, G. J., Maugeri, M., Mok, H. Y., Nordli, Ø., Ross, T. F., Trigo, R. M., Wang, X. L., Woodruff, S. D., and Worley, S. J.: The Twentieth Century Reanalysis Project, Quarterly Journal of the Royal Meteorological Society, 137, 1–28, https://doi.org/10.1002/qj.776, 2011.

Currie, L. A.: Nomenclature in Evaluation of Analytical Methods including Detection and Quantification Capabilities, Analytica Chimica Acta, 391, 105–126, https://doi.org/10.1016/S0003-2670(99)00104-X, 1999.

Dansgaard, W., Johnsen, S. J., Clausen, H. B., Dahl-Jensen, D., Gundestrup, N. S., Hammer, C. U., Hvidberg, C. S., Steffensen, J. P., Sveinbjörnsdottir, A. E., Jouzel, J., and Bond, G.: Evidence for general instability of past climate from a 250-kyr ice-core record, Nature, 364, 218–220, https://doi.org/10.1038/364218a0, 1993.

Davtian, N. and Bard, E.: A new view on abrupt climate changes and the bipolar seesaw based on paleotemperatures from Iberian Margin sediments, Proc. Natl. Acad. Sci. U.S.A., 120, e2209558120, https://doi.org/10.1073/pnas.2209558120, 2023.

Dawdy, D. and Matalas, N.: Analysis of variance, covariance, and time series: Chap. 8-III, Handbook of applied hydrology. New York: Mc Graw-Hill, 1964.

De Jonge, C., Hopmans, E. C., Zell, C. I., Kim, J. H., Schouten, S., and Sinninghe Damsté, J. S.: Occurrence and abundance of 6-methyl branched glycerol dialkyl glycerol tetraethers in soils: Implications for palaeoclimate reconstruction, Geochimica et Cosmochimica Acta, 141, 97–112, https://doi.org/10.1016/J.GCA.2014.06.013, 2014.

De Vernal, A., Rosell-Melé, A., Kucera, M., Hillaire-Marcel, C., Eynaud, F., Weinelt, M., Dokken, T., and Kageyama, M.: Comparing proxies for the reconstruction of LGM sea-surface conditions in the northern North Atlantic, Quaternary Science Reviews, 25, 2820–2834, https://doi.org/10.1016/j.quascirev.2006.06.006, 2006.

Dearing Crampton-Flood, E., Tierney, J. E., Peterse, F., Kirkels, F. M. S. A., and Sinninghe Damsté, J. S.: BayMBT: A Bayesian calibration model for branched glycerol dialkyl glycerol tetraethers in soils and peats, Geochimica et Cosmochimica Acta, 268, 142–159, https://doi.org/10.1016/J.GCA.2019.09.043, 2020.

Denton, G. H., Alley, R. B., Comer, G. C., and Broecker, W. S.: The role of seasonality in abrupt climate change, Quaternary Science Reviews, 24, 1159–1182, https://doi.org/10.1016/j.quascirev.2004.12.002, 2005.

Denton, G. H., Toucanne, S., Putnam, A. E., Barrell, D. J. A., and Russell, J. L.: Heinrich summers, Quaternary Science Reviews, 295, 107750, https://doi.org/10.1016/j.quascirev.2022.107750, 2022.

Duprat-Oualid, F., Rius, D., Bégeot, C., Magny, M., Millet, L., Wulf, S., and Appelt, O.: Vegetation response to abrupt climate changes in Western Europe from 45 to 14.7k cal a BP: the Bergsee lacustrine record (Black Forest, Germany), Journal of Quaternary Science, 32, 1008–1021, https://doi.org/10.1002/jqs.2972, 2017.

Fletcher, W. J., Sánchez Goñi, M. F., Allen, J. R. M., Cheddadi, R., Combourieu-Nebout, N., Huntley, B., Lawson, I., Londeix, L., Magri, D., Margari, V., Müller, U. C., Naughton, F., Novenko, E., Roucoux, K., and Tzedakis, P. C.: Millennial-scale variability during the last glacial in vegetation records from Europe, Quaternary Science Reviews, 29, 2839–2864, https://doi.org/10.1016/j.quascirev.2009.11.015, 2010.

Flückiger, J., Knutti, R., White, J. W. C., and Renssen, H.: Modeled seasonality of glacial abrupt climate events, Clim Dyn, 31, 633–645, https://doi.org/10.1007/s00382-008-0373-y, 2008.

Fuhrmann, F., Seelos, K., and Sirocko, F.: Eolian sedimentation in central European Auel dry maar from 60 to 13 ka, Quaternary Research, 101, 4–12, https://doi.org/10.1017/qua.2020.81, 2021.

Genty, D., Blamart, D., Ouahdi, R., Gilmour, M., Baker, A., Jouzel, J., and Van-Exter, S.: Precise dating of Dansgaard-Oeschger climate oscillations in western Europe from stalagmite data, Nature, 421, 833–837, https://doi.org/10.1038/nature01391, 2003.

Genty, D., Combourieu-Nebout, N., Peyron, O., Blamart, D., Wainer, K., Mansuri, F., Ghaleb, B., Isabello, L., Dormoy, I., von Grafenstein, U., Bonelli, S., Landais, A., and Brauer, A.: Isotopic characterization of rapid climatic events during OIS3 and OIS4 in Villars Cave stalagmites (SW-France) and correlation with Atlantic and Mediterranean pollen records, Quaternary Science Reviews, 29, 2799–2820, https://doi.org/10.1016/j.quascirev.2010.06.035, 2010.

Guiot, J., de Beaulieu, J. L., Cheddadi, R., David, F., Ponel, P., and Reille, M.: The climate in Western Europe during the last Glacial/Interglacial cycle derived from pollen and insect remains, Palaeogeography, Palaeoclimatology, Palaeoecology, 103, 73–93, https://doi.org/10.1016/0031-0182(93)90053-L, 1993.

Halamka, T. A., Raberg, J. H., McFarlin, J. M., Younkin, A. D., Mulligan, C., Liu, X., and Kopf, S. H.: Production of diverse brGDGTs by Acidobacterium Solibacter usitatus in response to temperature, pH, and O2 provides a culturing perspective on brGDGT proxies and biosynthesis, Geobiology, 21, 102–118, https://doi.org/10.1111/gbi.12525, 2023.

Heinrich, H.: Origin and Consequences of Cyclic Ice Rafting in the Northeast Atlantic Ocean During the Past 130,000 Years, Quat. res., 29, 142–152, https://doi.org/10.1016/0033-5894(88)90057-9, 1988.

Heiri, O., Brooks, S. J., Renssen, H., Bedford, A., Hazekamp, M., Ilyashuk, B., Jeffers, E. S., Lang, B., Kirilova, E., Kuiper, S., Millet, L., Samartin, S., Toth, M., Verbruggen, F., Watson, J. E., van Asch, N., Lammertsma, E., Amon, L., Birks, H. H., Birks, H. J. B., Mortensen, M. F., Hoek, W. Z., Magyari, E., Muñoz Sobrino, C., Seppä, H., Tinner, W., Tonkov, S., Veski, S., and Lotter, A. F.: Validation of climate model-inferred regional temperature change for late-glacial Europe, Nat Commun, 5, 4914, https://doi.org/10.1038/ncomms5914, 2014.

Heiri, O., Ilyashuk, B., Millet, L., Samartin, S., and Lotter, A. F.: Stacking of discontinuous regional palaeoclimate records: Chironomid-based summer temperatures from the Alpine region, Holocene, 25, 137–149, https://doi.org/10.1177/0959683614556382, 2015.

Helmens, K. F.: The last interglacial-glacial cycle (MIS 5-2) re-examined based on long proxy records from central and northern europe, Quaternary Science Reviews, 86, 115–143, https://doi.org/10.1016/j.quascirev.2013.12.012, 2014.

Hopmans, E. C., Weijers, J. W. H., Schefuß, E., Herfort, L., Sinninghe Damsté, J. S., and Schouten, S.: A novel proxy for terrestrial organic matter in sediments based on branched and isoprenoid tetraether lipids, Earth and Planetary Science Letters, 224, 107–116, https://doi.org/10.1016/j.epsl.2004.05.012, 2004.

700 Hopmans, E. C., Schouten, S., and Sinninghe Damsté, J. S.: The effect of improved chromatography on GDGT-based palaeoproxies, Organic Geochemistry, 93, 1–6, https://doi.org/10.1016/j.orggeochem.2015.12.006, 2016.

Jouzel, J., Masson-Delmotte, V., Cattani, O., Dreyfus, G., Falourd, S., Hoffmann, G., Minster, B., Nouet, J., Barnola, J. M., Chappellaz, J., Fischer, H., Gallet, J. C., Johnsen, S., Leuenberger, M., Loulergue, L., Luethi, D., Oerter, H., Parrenin, F., Raisbeck, G., Raynaud, D., Schilt, A., Schwander, J., Selmo, E., Souchez, R., Spahni, R., Stauffer, B., Steffensen, J. P., Stenni, 705 B., Stocker, T. F., Tison, J. L., Werner, M., and Wolff, E. W.: Orbital and Millennial Antarctic Climate Variability over the Past 800,000 Years, Science, 317, 793–796, https://doi.org/10.1126/science.1141038, 2007.

Kaufman, D., McKay, N., Routson, C., Erb, M., Dätwyler, C., Sommer, P. S., Heiri, O., and Davis, B.: Holocene global mean surface temperature, a multi-method reconstruction approach, Scientific Data, 7, 1–13, https://doi.org/10.1038/s41597-020-0530-7, 2020.

710 Kaufman, D. S. and Broadman, E.: Revisiting the Holocene global temperature conundrum, Nature, 614, 425–435, https://doi.org/10.1038/s41586-022-05536-w, 2023.

Kindler, P., Guillevic, M., Baumgartner, M., Schwander, J., Landais, A., and Leuenberger, M.: Temperature reconstruction from 10 to 120 kyr b2k from the NGRIP ice core, Clim. Past, 10, 887–902, https://doi.org/10.5194/cp-10-887-2014, 2014.

Kobashi, T., Menviel, L., Jeltsch-Thömmes, A., Vinther, B. M., Box, J. E., Muscheler, R., Nakaegawa, T., Pfister, P. L., 715 Döring, M., Leuenberger, M., Wanner, H., and Ohmura, A.: Volcanic influence on centennial to millennial Holocene Greenland temperature change, Sci Rep, 7, 1441, https://doi.org/10.1038/s41598-017-01451-7, 2017.

Kwiecien, O., Braun, T., Brunello, C. F., Faulkner, P., Hausmann, N., Helle, G., Hoggarth, J. A., Ionita, M., Jazwa, C., Kelmelis, S., Marwan, N., Nava-Fernandez, C., Nehme, C., Opel, T., Oster, J. L., Perşoiu, A., Petrie, C., Prufer, K., Saarni, S. M., Wolf, A., and Breitenbach, S. F. M.: What we talk about when we talk about seasonality – A transdisciplinary review, 720 Earth-Science Reviews, 103843, https://doi.org/10.1016/J.EARSCIREV.2021.103843, 2021.

Laskar, J., Robutel, P., Joutel, F., Gastineau, M., Correia, A. C. M., and Levrard, B.: A long-term numerical solution for the insolation quantities of the Earth, Astronomy & Astrophysics, 428, 261–285, https://doi.org/10.1051/0004-6361:20041335, 2004.

Leonardi, M., Hallett, E. Y., Beyer, R., Krapp, M., and Manica, A.: pastclim 1.2: an R package to easily access and use 725 paleoclimatic reconstructions, Ecography, 2023, e06481, https://doi.org/10.1111/ecog.06481, 2023.

Loomis, S. E., Russell, J. M., Heureux, A. M., D'Andrea, W. J., and Sinninghe Damsté, J. S.: Seasonal variability of branched glycerol dialkyl glycerol tetraethers (brGDGTs) in a temperate lake system, Geochimica et Cosmochimica Acta, 144, 173–187, https://doi.org/10.1016/j.gca.2014.08.027, 2014.

Lücke, A., Schleser, G. H., Zolitschka, B., and Negendank, J. F. W.: A Lateglacial and Holocene organic carbon isotope record 730 of lacustrine palaeoproductivity and climatic change derived from varved lake sediments of Lake Holzmaar, Germany, Quaternary Science Reviews, 22, 569–580, https://doi.org/10.1016/S0277-3791(02)00187-7, 2003.

Martin, C., Ménot, G., Thouveny, N., Davtian, N., Andrieu-Ponel, V., Reille, M., and Bard, E.: Impact of human activities and vegetation changes on the tetraether sources in Lake St Front (Massif Central, France), Organic Geochemistry, 135, 38–52, https://doi.org/10.1016/J.ORGGEOCHEM.2019.06.005, 2019.

Martin, C., Ménot, G., Thouveny, N., Peyron, O., Andrieu-Ponel, V., Montade, V., Davtian, N., Reille, M., and Bard, E.: Early Holocene Thermal Maximum recorded by branched tetraethers and pollen in Western Europe (Massif Central, France), Quaternary Science Reviews, 228, 106109, https://doi.org/10.1016/j.quascirev.2019.106109, 2020.

Martínez-Sosa, P. and Tierney, J. E.: Lacustrine brGDGT response to microcosm and mesocosm incubations, Organic Geochemistry, 127, 12–22, https://doi.org/10.1016/J.ORGGEOCHEM.2018.10.011, 2019.

Martínez-Sosa, P., Tierney, J. E., and Meredith, L. K.: Controlled lacustrine microcosms show a brGDGT response to environmental perturbations, Organic Geochemistry, 145, https://doi.org/10.1016/J.ORGGEOCHEM.2020.104041, 2020.

Martínez-Sosa, P., Tierney, J. E., Stefanescu, I. C., Dearing Crampton-Flood, E., Shuman, B. N., and Routson, C.: A global Bayesian temperature calibration for lacustrine brGDGTs, Geochimica et Cosmochimica Acta, 305, 87–105, https://doi.org/10.1016/j.gca.2021.04.038, 2021.

Martínez-Sosa, P., Tierney, J. E., Pérez-Angel, L. C., Stefanescu, I. C., Guo, J., Kirkels, F., Sepúlveda, J., Peterse, F., Shuman, B. N., and Reyes, A. V.: Development and application of the Branched and Isoprenoid GDGT Machine learning Classification algorithm (BIGMaC) for paleoenvironmental reconstruction, Paleoceanography and Paleoclimatology, n/a, e2023PA004611, https://doi.org/10.1029/2023PA004611, 2023.

Martrat, B., Grimalt, J. O., Shackleton, N. J., De Abreu, L., Hutterli, M. A., and Stocker, T. F.: Four climate cycles of recurring deep and surface water destabilizations on the Iberian margin, Science, 317, 502–507, https://doi.org/10.1126/science.1139994, 2007.

Mauri, A., Davis, B. A. S., Collins, P. M., and Kaplan, J. O.: The climate of Europe during the Holocene: A gridded pollen-based reconstruction and its multi-proxy evaluation, Quaternary Science Reviews, 112, 109–127, https://doi.org/10.1016/J.QUASCIREV.2015.01.013, 2015.

Mckay, N. P., Emile-Geay, J., and Khider, D.: GeoChronR - An R package to model, analyze, and visualize age-uncertain data, Geochronology, 3, 149–169, https://doi.org/10.5194/GCHRON-3-149-2021, 2021.

Menviel, L. C., Skinner, L. C., Tarasov, L., and Tzedakis, P. C.: An ice–climate oscillatory framework for Dansgaard–Oeschger cycles, Nat Rev Earth Environ, 1, 677–693, https://doi.org/10.1038/s43017-020-00106-y, 2020.

Moreno, A., Svensson, A., Brooks, S. J., Connor, S., Engels, S., Fletcher, W., Genty, D., Heiri, O., Labuhn, I., Perşoiu, A., Peyron, O., Sadori, L., Valero-Garcés, B., Wulf, S., Zanchetta, G., Allen, J. R. M., Ampel, L., Blamart, D., Birks, H., Blockley, S., Borsato, A., Bos, H., Brauer, A., Combourieu-Nebout, N., de Beaulieu, J. L., Drescher-Schneider, R., Drysdale, R., Elias, S., Frisia, S., Hellstrom, J. C., Ilyashuk, B., Joannin, S., Kühl, N., Larocque-Tobler, I., Lotter, A., Magny, M., Matthews, I., McDermott, F., Millet, L., Morellón, M., Neugebauer, I., Muñoz-Sobrino, C., Naughton, F., Ohlwein, C., Roucoux, K., Samartin, S., Sánchez-Goñi, M. F., Sirocko, F., van Asch, N., van Geel, B., van Grafenstein, U., Vannière, B., Vegas, J., Veres, D., Walker, M., and Wohlfarth, B.: A compilation of Western European terrestrial records 60-8kaBP: Towards an understanding of latitudinal climatic gradients, Quaternary Science Reviews, 106, 167–185, https://doi.org/10.1016/j.quascirev.2014.06.030, 2014.

Moseley, G. E., Spötl, C., Svensson, A., Cheng, H., Brandstätter, S., and Edwards, R. L.: Multi-speleothem record reveals tightly coupled climate between central europe and greenland during marine isotope stage 3, Geology, 42, 1043–1046, https://doi.org/10.1130/G36063.1, 2014.

Naafs, B. D. A., Inglis, G. N., Zheng, Y., Amesbury, M. J., Biester, H., Bindler, R., Blewett, J., Burrows, M. A., del Castillo Torres, D., Chambers, F. M., Cohen, A. D., Evershed, R. P., Feakins, S. J., Gałka, M., Gallego-Sala, A., Gandois, L., Gray, D. M., Hatcher, P. G., Honorio Coronado, E. N., Hughes, P. D. M., Huguet, A., Könönen, M., Laggoun-Défarge, F., Lähteenoja,

O., Lamentowicz, M., Marchant, R., McClymont, E., Pontevedra-Pombal, X., Ponton, C., Pourmand, A., Rizzuti, A. M.,
Rochefort, L., Schellekens, J., De Vleeschouwer, F., and Pancost, R. D.: Introducing global peat-specific temperature and pH
calibrations based on brGDGT bacterial lipids, Geochimica et Cosmochimica Acta, 208, 285–301,
https://doi.org/10.1016/j.gca.2017.01.038, 2017.

North Greenland Ice Core Project members: High-resolution record of Northern Hemisphere climate extending into the last
interglacial period, Nature, 431, 147–151, https://doi.org/10.1038/nature02805, 2004.

Osborn, T. J. and Jones, P. D.: The CRUTEM4 land-surface air temperature data set: construction, previous versions and
dissemination via Google Earth, Earth System Science Data, 6, 61–68, https://doi.org/10.5194/essd-6-61-2014, 2014.

Parish, M. C., Du, X., Bijaksana, S., and Russell, J. M.: A brGDGT-Based Reconstruction of Terrestrial Temperature From
the Maritime Continent Spanning the Last Glacial Maximum, Paleoceanography and Paleoclimatology, 38, e2022PA004501,
https://doi.org/10.1029/2022PA004501, 2023.

Patwardhan, A. P. and Thompson, D. H.: Efficient Synthesis of 40- and 48-Membered Tetraether Macrocyclic
Bisphosphocholines, Org. Lett., 1, 241–244, https://doi.org/10.1021/ol990567o, 1999.

Peaple, M. D., Bhattacharya, T., Lowenstein, T. K., McGee, D., Olson, K. J., Stroup, J. S., Tierney, J. E., and Feakins, S. J.:
Biomarker and Pollen Evidence for Late Pleistocene Pluvials in the Mojave Desert, Paleoceanography and Paleoclimatology,
37, e2022PA004471, https://doi.org/10.1029/2022PA004471, 2022.

Prud'homme, C., Fischer, P., Jöris, O., Gromov, S., Vinnepand, M., Hatté, C., Vonhof, H., Moine, O., Vött, A., and
Fitzsimmons, K. E.: Millennial-timescale quantitative estimates of climate dynamics in central Europe from earthworm calcite
granules in loess deposits, Commun Earth Environ, 3, 1–14, https://doi.org/10.1038/s43247-022-00595-3, 2022.

R Core Team: R: A Language and Environment for Statistical Computing, 2022.

Raberg, J. H., Harning, D. J., Crump, S. E., De Wet, G., Blumm, A., Kopf, S., Geirsdóttir, Á., Miller, G. H., and Sepúlveda,
J.: Revised fractional abundances and warm-season temperatures substantially improve brGDGT calibrations in lake
sediments, Biogeosciences, 18, 3579–3603, https://doi.org/10.5194/bg-18-3579-2021, 2021.

Raberg, J. H., Miller, G. H., Geirsdóttir, Á., and Sepúlveda, J.: Near-universal trends in brGDGT lipid distributions in nature,
Science Advances, 8, 7625, https://doi.org/10.1126/SCIADV.ABM7625, 2022.

Ramos-Román, M. J., De Jonge, C., Magyari, E., Veres, D., Ilvonen, L., Develle, A.-L., and Seppä, H.: Lipid biomarker
(brGDGT)- and pollen-based reconstruction of temperature change during the Middle to Late Holocene transition in the
Carpathians, Global and Planetary Change, 215, 103859, https://doi.org/10.1016/j.gloplacha.2022.103859, 2022.

Rasmussen, S. O., Bigler, M., Blockley, S. P., Blunier, T., Buchardt, S. L., Clausen, H. B., Cvijanovic, I., Dahl-Jensen, D.,
Johnsen, S. J., Fischer, H., Gkinis, V., Guillevic, M., Hoek, W. Z., Lowe, J. J., Pedro, J. B., Popp, T., Seierstad, I. K., Steffensen,
J. P., Svensson, A. M., Vallelonga, P., Vinther, B. M., Walker, M. J. C., Wheatley, J. J., and Winstrup, M.: A stratigraphic
framework for abrupt climatic changes during the Last Glacial period based on three synchronized Greenland ice-core records:
Refining and extending the INTIMATE event stratigraphy, Quaternary Science Reviews, 106, 14–28,
https://doi.org/10.1016/j.quascirev.2014.09.007, 2014.

Renssen, H., Seppä, H., Heiri, O., Roche, D. M., Goosse, H., and Fichefet, T.: The spatial and temporal complexity of the
Holocene thermal maximum, Nature Geosci, 2, 411–414, https://doi.org/10.1038/ngeo513, 2009.

810   Riechelmann, D. F. C., Albert, J., Britzius, S., Krebsbach, F., Scholz, D., Schenk, F., Jochum, K. P., and Sirocko, F.: Bioproductivity and vegetation changes documented in Eifel maar lake sediments (western Germany) compared with speleothem growth indicating three warm phases during the last glacial cycle, Quaternary International, https://doi.org/10.1016/j.quaint.2023.11.001, 2023.

Russell, J. M., Hopmans, E. C., Loomis, S. E., Liang, J., and Sinninghe Damsté, J. S.: Distributions of 5- and 6-methyl branched
815   glycerol dialkyl glycerol tetraethers (brGDGTs) in East African lake sediment: Effects of temperature, pH, and new lacustrine paleotemperature calibrations, Organic Geochemistry, 117, 56–69, https://doi.org/10.1016/J.ORGGEOCHEM.2017.12.003, 2018.

Sánchez Goñi, M., Cacho, I., Turon, J., Guiot, J., Sierro, F., Peypouquet, J., Grimalt, J., and Shackleton, N.: Synchroneity between marine and terrestrial responses to millennial scale climatic variability during the last glacial period in the
820   Mediterranean region, Climate Dynamics, 19, 95–105, https://doi.org/10.1007/s00382-001-0212-x, 2002.

Sánchez Goñi, M. F., Turon, J.-L., Eynaud, F., and Gendreau, S.: European Climatic Response to Millennial-Scale Changes in the Atmosphere–Ocean System during the Last Glacial Period, Quaternary Research, 54, 394–403, https://doi.org/10.1006/qres.2000.2176, 2000.

Sánchez Goñi, M. F., Landais, A., Fletcher, W. J., Naughton, F., Desprat, S., and Duprat, J.: Contrasting impacts of Dansgaard–
825   Oeschger events over a western European latitudinal transect modulated by orbital parameters, Quaternary Science Reviews, 27, 1136–1151, https://doi.org/10.1016/j.quascirev.2008.03.003, 2008.

Sánchez Goñi, M. F., Fourcade, T., Salonen, S., Lesven, J., Frigola, J., Swingedouw, D., and Sierro, F. J.: Muted cooling and drying of NW Mediterranean in response to the strongest last glacial North American ice surges, GSA Bulletin, 133, 451–460, https://doi.org/10.1130/B35736.1, 2021.

830   Schmincke, H.-U.: The Quaternary Volcanic Fields of the East and West Eifel (Germany), in: Mantle Plumes: A Multidisciplinary Approach, edited by: Ritter, J. R. R. and Christensen, U. R., Springer, Berlin, Heidelberg, 241–322, https://doi.org/10.1007/978-3-540-68046-8_8, 2007.

Schouten, S., Hopmans, E. C., and Sinninghe Damsté, J. S.: The organic geochemistry of glycerol dialkyl glycerol tetraether lipids: A review, Organic Geochemistry, 54, 19–61, https://doi.org/10.1016/j.orggeochem.2012.09.006, 2013.

835   Seguinot, J., Ivy-Ochs, S., Jouvet, G., Huss, M., Funk, M., and Preusser, F.: Modelling last glacial cycle ice dynamics in the Alps, The Cryosphere, 12, 3265–3285, https://doi.org/10.5194/tc-12-3265-2018, 2018.

Sinninghe Damsté, J. S., Rijpstra, W. I. C., Hopmans, E. C., Weijers, J. W. H., Foesel, B. U., Overmann, J., and Dedysh, S. N.: 13,16-Dimethyl Octacosanedioic Acid (iso-Diabolic Acid), a Common Membrane-Spanning Lipid of Acidobacteria Subdivisions 1 and 3, Applied and Environmental Microbiology, 77, 4147–4154, https://doi.org/10.1128/AEM.00466-11,
840   2011.

Sinninghe Damsté, J. S., Rijpstra, W. I. C., Hopmans, E. C., Jung, M.-Y., Kim, J.-G., Rhee, S.-K., Stieglmeier, M., and Schleper, C.: Intact Polar and Core Glycerol Dibiphytanyl Glycerol Tetraether Lipids of Group I.1a and I.1b Thaumarchaeota in Soil, Applied and Environmental Microbiology, 78, 6866–6874, https://doi.org/10.1128/AEM.01681-12, 2012.

Sinninghe Damsté, J. S., Weber, Y., Zopfi, J., Lehmann, M. F., and Niemann, H.: Distributions and sources of isoprenoidal
845   GDGTs in Lake Lugano and other central European (peri-)alpine lakes: Lessons for their use as paleotemperature proxies, Quaternary Science Reviews, 277, 107352, https://doi.org/10.1016/J.QUASCIREV.2021.107352, 2022.

Sirocko, F. (Ed.): Wetter, Klima, Menschheitsentwicklung: von der Eiszeit bis ins 21. Jahrhundert, 3., durchgesehene Auflage., Konrad Theiss Verlag, Stuttgart, 208 pp., 2012.

850 Sirocko, F.: The ELSA - Stacks (Eifel-Laminated-Sediment-Archive): An introduction, Global and Planetary Change, 142, 96–99, https://doi.org/10.1016/j.gloplacha.2016.03.011, 2016.

Sirocko, F., Knapp, H., Dreher, F., Förster, M. W., Albert, J., Brunck, H., Veres, D., Dietrich, S., Zech, M., Hambach, U., Röhner, M., Rudert, S., Schwibus, K., Adams, C., and Sigl, P.: The ELSA-Vegetation-Stack: Reconstruction of Landscape Evolution Zones (LEZ) from laminated Eifel maar sediments of the last 60,000 years, Global and Planetary Change, 142, 108–135, https://doi.org/10.1016/j.gloplacha.2016.03.005, 2016.

855 Sirocko, F., Martínez-García, A., Mudelsee, M., Albert, J., Britzius, S., Christl, M., Diehl, D., Diensberg, B., Friedrich, R., Fuhrmann, F., Muscheler, R., Hamann, Y., Schneider, R., Schwibus, K., and Haug, G. H.: Muted multidecadal climate variability in central Europe during cold stadial periods, Nature Geoscience, 14, 651–658, https://doi.org/10.1038/s41561-021-00786-1, 2021.

Sirocko, F., Albert, J., Britzius, S., Dreher, F., Martínez-García, A., Dosseto, A., Burger, J., Terberger, T., and Haug, G.: 860 Thresholds for the presence of glacial megafauna in central Europe during the last 60,000 years, Sci Rep, 12, 20055, https://doi.org/10.1038/s41598-022-22464-x, 2022.

Slivinski, L. C., Compo, G. P., Whitaker, J. S., Sardeshmukh, P. D., Giese, B. S., McColl, C., Allan, R., Yin, X., Vose, R., Titchner, H., Kennedy, J., Spencer, L. J., Ashcroft, L., Brönnimann, S., Brunet, M., Camuffo, D., Cornes, R., Cram, T. A., Crouthamel, R., Domínguez-Castro, F., Freeman, J. E., Gergis, J., Hawkins, E., Jones, P. D., Jourdain, S., Kaplan, A., Kubota, 865 H., Blancq, F. L., Lee, T.-C., Lorrey, A., Luterbacher, J., Maugeri, M., Mock, C. J., Moore, G. W. K., Przybylak, R., Pudmenzky, C., Reason, C., Slonosky, V. C., Smith, C. A., Tinz, B., Trewin, B., Valente, M. A., Wang, X. L., Wilkinson, C., Wood, K., and Wyszyński, P.: Towards a more reliable historical reanalysis: Improvements for version 3 of the Twentieth Century Reanalysis system, Quarterly Journal of the Royal Meteorological Society, 145, 2876–2908, https://doi.org/10.1002/qj.3598, 2019.

870 Spötl, C. and Mangini, A.: Stalagmite from the Austrian Alps reveals Dansgaard-Oeschger events during isotope stage 3: Implications for the absolute chronology of Greenland ice cores, Earth and Planetary Science Letters, 203, 507–518, https://doi.org/10.1016/S0012-821X(02)00837-3, 2002.

Stefanescu, I. C., Shuman, B. N., and Tierney, J. E.: Temperature and water depth effects on brGDGT distributions in sub-alpine lakes of mid-latitude North America, Organic Geochemistry, 152, 104174, 875 https://doi.org/10.1016/J.ORGGEOCHEM.2020.104174, 2021.

Thompson, A. J., Zhu, J., Poulsen, C. J., Tierney, J. E., and Skinner, C. B.: Northern Hemisphere vegetation change drives a Holocene thermal maximum, Science Advances, 8, eabj6535, https://doi.org/10.1126/SCIADV.ABJ6535, 2022.

Tierney, J. E. and Russell, J. M.: Distributions of branched GDGTs in a tropical lake system: Implications for lacustrine application of the MBT/CBT paleoproxy, Organic Geochemistry, 40, 1032–1036, 880 https://doi.org/10.1016/j.orggeochem.2009.04.014, 2009.

Tierney, J. E., Russell, J. M., Eggermont, H., Hopmans, E. C., Verschuren, D., and Sinninghe Damsté, J. S.: Environmental controls on branched tetraether lipid distributions in tropical East African lake sediments, Geochimica et Cosmochimica Acta, 74, 4902–4918, https://doi.org/10.1016/j.gca.2010.06.002, 2010.

Tierney, J. E., Zhu, J., King, J., Malevich, S. B., Hakim, G. J., and Poulsen, C. J.: Glacial cooling and climate sensitivity 885 revisited, Nature, 584, 569–573, https://doi.org/10.1038/s41586-020-2617-x, 2020.

Toucanne, S., Soulet, G., Freslon, N., Silva Jacinto, R., Dennielou, B., Zaragosi, S., Eynaud, F., Bourillet, J.-F., and Bayon, G.: Millennial-scale fluctuations of the European Ice Sheet at the end of the last glacial, and their potential impact on global climate, Quaternary Science Reviews, 123, 113–133, https://doi.org/10.1016/j.quascirev.2015.06.010, 2015.

890 Újvári, G., Stevens, T., Molnár, M., Demény, A., Lambert, F., Varga, G., Jull, A. J. T., Páll-Gergely, B., Buylaert, J.-P., and Kovács, J.: Coupled European and Greenland last glacial dust activity driven by North Atlantic climate, Proceedings of the National Academy of Sciences, 114, E10632–E10638, https://doi.org/10.1073/pnas.1712651114, 2017.

Újvári, G., Bernasconi, S. M., Stevens, T., Kele, S., Páll-Gergely, B., Surányi, G., and Demény, A.: Stadial-Interstadial Temperature and Aridity Variations in East Central Europe Preceding the Last Glacial Maximum, Paleoceanography and Paleoclimatology, 36, e2020PA004170, https://doi.org/10.1029/2020PA004170, 2021.

895 Van Bree, L. G. J., Peterse, F., Baxter, A. J., De Crop, W., Van Grinsven, S., Villanueva, L., Verschuren, D., and Sinninghe Damsté, J. S.: Seasonal variability and sources of in situ brGDGT production in a permanently stratified African crater lake, Biogeosciences, 17, 5443–5463, https://doi.org/10.5194/BG-17-5443-2020, 2020.

Van Meerbeeck, C. J., Renssen, H., Roche, D. M., Wohlfarth, B., Bohncke, S. J. P., Bos, J. A. A., Engels, S., Helmens, K. F., Sánchez-Goñi, M. F., Svensson, A., and Vandenberghe, J.: The nature of MIS 3 stadial-interstadial transitions in Europe: New
900 insights from model-data comparisons, Quaternary Science Reviews, 30, 3618–3637, https://doi.org/10.1016/j.quascirev.2011.08.002, 2011.

Véquaud, P., Thibault, A., Derenne, S., Anquetil, C., Collin, S., Contreras, S., Nottingham, A. T., Sabatier, P., Werne, J. P., and Huguet, A.: FROG: A global machine-learning temperature calibration for branched GDGTs in soils and peats, Geochimica et Cosmochimica Acta, 318, 468–494, https://doi.org/10.1016/J.GCA.2021.12.007, 2022.

905 Wang, H., Liu, W., He, Y., Zhou, A., Zhao, H., Liu, H., Cao, Y., Hu, J., Meng, B., Jiang, J., Kolpakova, M., Krivonogov, S., and Liu, Z.: Salinity-controlled isomerization of lacustrine brGDGTs impacts the associated MBT5ME' terrestrial temperature index, Geochimica et Cosmochimica Acta, 305, 33–48, https://doi.org/10.1016/j.gca.2021.05.004, 2021.

Wang, H., Chen, W., Zhao, H., Cao, Y., Hu, J., Zhao, Z., Cai, Z., Wu, S., Liu, Z., and Liu, W.: Biomarker-based quantitative constraints on maximal soil-derived brGDGTs in modern lake sediments, Earth and Planetary Science Letters, 602, 117947,
910 https://doi.org/10.1016/j.epsl.2022.117947, 2023.

Weber, Y., De Jonge, C., Rijpstra, W. I. C., Hopmans, E. C., Stadnitskaia, A., Schubert, C. J., Lehmann, M. F., Sinninghe Damsté, J. S., and Niemann, H.: Identification and carbon isotope composition of a novel branched GDGT isomer in lake sediments: Evidence for lacustrine branched GDGT production, Geochimica et Cosmochimica Acta, 154, 118–129, https://doi.org/10.1016/J.GCA.2015.01.032, 2015.

915 Weber, Y., Damsté, J. S. S., Zopfi, J., De Jonge, C., Gilli, A., Schubert, C. J., Lepori, F., Lehmann, M. F., and Niemann, H.: Redox-dependent niche differentiation provides evidence for multiple bacterial sources of glycerol tetraether lipids in lakes, Proceedings of the National Academy of Sciences of the United States of America, 115, 10926–10931, https://doi.org/10.1073/pnas.1805186115, 2018.

Weijers, J. W. H., Schouten, S., van den Donker, J. C., Hopmans, E. C., and Sinninghe Damsté, J. S.: Environmental controls
920 on bacterial tetraether membrane lipid distribution in soils, Geochimica et Cosmochimica Acta, 71, 703–713, https://doi.org/10.1016/j.gca.2006.10.003, 2007.

Wohlfarth, B., Veres, D., Ampel, L., Lacourse, T., Blaauw, M., Preusser, F., Andrieu-Ponel, V., Kéravis, D., Lallier-Vergès, E., Björck, S., Davies, S. M., de Beaulieu, J.-L., Risberg, J., Hormes, A., Kasper, H. U., Possnert, G., Reille, M., Thouveny,

N., and Zander, A.: Rapid ecosystem response to abrupt climate changes during the last glacial period in western Europe, 40–
925 16 ka, Geology, 36, 407–410, https://doi.org/10.1130/G24600A.1, 2008.

Xiao, W., Wang, Y., Zhou, S., Hu, L., Yang, H., and Xu, Y.: Ubiquitous production of branched glycerol dialkyl glycerol
tetraethers (brGDGTs) in global marine environments: a new source indicator for brGDGTs, Biogeosciences, 13, 5883–5894,
https://doi.org/10.5194/bg-13-5883-2016, 2016.

Zhao, B., Castañeda, I. S., Bradley, R. S., Salacup, J. M., de Wet, G. A., Daniels, W. C., and Schneider, T.: Development of
930 an in situ branched GDGT calibration in Lake 578, southern Greenland, Organic Geochemistry, 152, 104168,
https://doi.org/10.1016/J.ORGGEOCHEM.2020.104168, 2021.